

# Path Weight Sampling: Exact Monte Carlo Computation of the Mutual Information between Stochastic Trajectories

Manuel Reinhardt,<sup>1</sup> Gašper Tkačik,<sup>2</sup> and Pieter Rein ten Wolde<sup>1,\*</sup>

<sup>1</sup>*AMOLF, Science Park 104, 1098 XG, Amsterdam, The Netherlands*

<sup>2</sup>*Institute of Science and Technology Austria, 3400 Klosterneuburg, Austria*

(Dated: March 8, 2022)

Most natural and engineered information-processing systems transmit information via signals that vary in time. Computing the information transmission rate or the information encoded in the temporal characteristics of these signals, requires the mutual information between the input and output signals as a function of time, i.e. between the input and output trajectories. Yet, this is notoriously difficult because of the high-dimensional nature of the trajectory space, and all existing techniques require approximations. We present an exact Monte Carlo technique called *Path Weight Sampling* (PWS) that, for the first time, makes it possible to compute the mutual information between input and output trajectories for any stochastic system that is described by a master equation. The principal idea is to use the master equation to evaluate the exact conditional probability of an individual output trajectory for a given input trajectory, and average this via Monte Carlo sampling in trajectory space to obtain the mutual information. We present three variants of PWS, which all generate the trajectories using the standard stochastic simulation algorithm. While *Direct PWS* is a brute-force method, *Rosenbluth-Rosenbluth PWS* exploits the analogy between signal trajectory sampling and polymer sampling, and *Thermodynamic Integration PWS* is based on a reversible work calculation in trajectory space. PWS also makes it possible to compute the mutual information between input and output trajectories for systems with hidden internal states as well as systems with feedback from output to input. Applying PWS to the bacterial chemotaxis system, consisting of 173 coupled chemical reactions, demonstrates not only that the scheme is highly efficient, but also that the appropriate measure for quantifying information transmission via time-varying signals is indeed the information transmission rate.

Keywords: Complex Systems, Statistical Physics, Computational Physics

## I. INTRODUCTION

Quantifying information transmission is vital for understanding and designing natural and engineered information-processing systems, ranging from biochemical and neural networks, to electronic circuits and optical systems [1–3]. Claude Shannon introduced the mutual information and the information rate as the central measures of Information Theory more than 70 years ago [4]. These measures quantify the fidelity by which a noisy system transmits information from its inputs to its outputs. Yet, computing these quantities exactly remains notoriously difficult, if not impossible. This is because the inputs and outputs are often not scalar values, but rather temporal *trajectories*.

Most, if not all, information-processing systems transmit signal that vary in time. The canonical measure for quantifying information transmission via time-varying signals is the mutual information rate [4–7]. It quantifies the speed at which distinct messages are transmitted through the system, and it depends not only on the accuracy of the input-output mapping but also on the correlations within the input and output signals. Taking these correlations into account requires computing the mutual information between the input and output trajectories, not between their signal values at given time

points; the rate at which this trajectory mutual information increases with the trajectory duration in the long-time limit defines the mutual information rate. In the absence of feedback this rate also equals the multi-step transfer entropy [8, 9].

More generally, the information is often contained in the temporal dynamics of the signal. A prime example is bacterial chemotaxis, where the response does not depend on the current ligand concentration, but rather on whether it has changed in the recent past [10, 11]. Moreover, the information from the input may be encoded in the temporal dynamics of the output [12–15]. Quantifying information encoded in these temporal features of the signals requires the mutual information not between two time points, i.e. the instantaneous mutual information, but rather between input and output trajectories [6].

Unfortunately, computing the mutual information between trajectories is exceptionally difficult. The conventional approach requires non-parametric distribution estimates of the input and output distributions, e.g. via histograms of data obtained through simulations or experiments [16–21]. These non-parametric distribution estimates are necessary because the mutual information cannot generally be computed from summary statistics like the mean or variance of the data alone. However, the high-dimensional nature of trajectories makes it infeasible to obtain enough empirical data to accurately estimate the required probability distributions. Moreover, this approach requires the discretization of time, which

\* tenwolde@amolf.nl

becomes problematic when the information is encoded in the precise timing of signal spikes, as, e.g., in neuronal systems [22]. Except for the simplest systems with a binary state space [21], the conventional approach to estimate the mutual information via histograms therefore cannot be transposed to trajectories.

Because there are currently no general schemes available to compute the mutual information between trajectories exactly, approximate methods or simplified models are typically used. While empirical distribution estimates can be avoided by employing the K-nearest-neighbors entropy estimator [23, 24], this method depends on a choice of metric in trajectory space and can become unreliable for long trajectories [25]. Analytically, the mutual information between trajectories can only be obtained for linear models that assume Gaussian statistics of the input and the output [6] and other similarly simple systems [26]. However, many information processing systems are complex and non-linear such that the Gaussian approximation does not hold, and analytical solutions do not exist. Alternative, decoding-based information estimates can be developed for trajectories [27], but merely provide a lower bound of the mutual information, and it remains unclear how tight these lower bounds are [25, 28, 29]. A more promising approach to estimate the trajectory mutual information for chemical reaction networks has been developed by Duso and Zechner [30]. However, their scheme relies on a moment closure approximation and has so far only been applied to very simple networks, seemingly being difficult to extend to complex systems.

Here, we present *Path Weight Sampling* (PWS), an *exact* technique to compute the trajectory mutual information for any system described by a master equation. Master equations are widely used to model chemical reaction networks [31–34], biological population growth [35–37], economic processes [38, 39], and a large variety of other systems [40, 41], making our scheme of interest to a broad class of problems. In PWS, the mutual information is computed as the difference between the marginal output entropy associated with the marginal distribution  $\mathcal{P}[\mathbf{x}]$  of the output trajectories  $\mathbf{x}$ , and the conditional output entropy associated with the output distribution  $\mathcal{P}[\mathbf{x}|\mathbf{s}]$  conditioned on the input trajectory  $\mathbf{s}$ . Our scheme is inspired by the observation from Cepeda-Humerez *et al.* [25] that the path likelihood, i.e. the probability  $\mathcal{P}[\mathbf{x}|\mathbf{s}]$ , can be computed exactly from the master equation for a *static* input signal  $s$ . This makes it possible to compute the mutual information between a discrete input and a time-varying output via a Monte Carlo averaging procedure of the likelihoods, rather than from an empirical estimate of the intractable high-dimensional probability distribution functions. The scheme of Cepeda-Humerez *et al.* [25] is however limited to discrete input signals that do not vary in time. Here we show that the path likelihood  $\mathcal{P}[\mathbf{x}|\mathbf{s}]$  can also be computed for an input *trajectory*  $\mathbf{s}$ , which allows us to compute the conditional output entropy also for time-varying inputs. While this solves

the problem in part, the marginal output entropy associated with  $\mathcal{P}[\mathbf{x}]$  cannot be computed with the approach of Cepeda-Humerez *et al.*, and thus requires a different scheme.

We show how, for time-varying input signals, the marginal probability  $\mathcal{P}[\mathbf{x}]$  of a given output trajectory  $\mathbf{x}$  can be obtained via Monte Carlo schemes, by averaging  $\mathcal{P}[\mathbf{x}|\mathbf{s}]$  over a large number of input trajectories, which then allows us to compute the marginal output entropy. We present three variants of PWS, all of which compute the conditional entropy in the same manner, but differ in the way this Monte Carlo averaging procedure for computing the marginal probability  $\mathcal{P}[\mathbf{x}]$  is carried out.

To compute  $\mathcal{P}[\mathbf{x}]$ , *Direct* PWS (DPWS) performs a brute-force average of the path likelihoods  $\mathcal{P}[\mathbf{x}|\mathbf{s}]$  over the input trajectories  $\mathbf{s}$ . While we show that this scheme works for simple systems, the brute-force Monte Carlo averaging procedure becomes more difficult for larger systems and exponentially harder for longer trajectories.

Our second and third variant of PWS are based on the realization that the marginal probability  $\mathcal{P}[\mathbf{x}]$  is akin to a partition function. These schemes leverage techniques for computing free energies from statistical physics, drawing on ideas from path sampling and capitalizing on the analogy between signal trajectory sampling and polymer sampling. Specifically, the second scheme, *Rosenbluth-Rosenbluth PWS* (RR-PWS), exploits the observation that the computation of  $\mathcal{P}[\mathbf{x}]$  is analogous to the calculation of the (excess) chemical potential of a polymer, for which efficient methods have been developed [42–44]. The third scheme, *Thermodynamic Integration PWS* (TI-PWS), is based on the classic free energy estimation technique of thermodynamic integration [45–47] in conjunction with a trajectory space MCMC sampler using ideas from transition path sampling [48].

All three PWS variants make it possible to exactly compute the mutual information between trajectories without the need to time-discretize the input and output signals and fill the corresponding high-dimensional histograms.

The DPWS method is presented in Section II, followed by a review of the required concepts from the theory of Markov jump processes and master equations. The other two PWS schemes are then presented as improvements of DPWS in Section III.

In Section IV we show that, surprisingly, our PWS methods additionally make it possible to compute the mutual information between input and output trajectories of systems with hidden internal states. Hidden states correspond, for example, to network components that merely relay or process, i.e. (non-)linearly transform, the signal from the input to the output. Indeed, the downstream system typically responds to the information that is encoded in this output, and not the other system components. Most, if not all, complex information processing devices contain such hidden states, and generally we want to integrate out these latent network components. Other important applications are state-space and, in particular,

hidden Markov models (HMM), which are inferred from experimental data [49, 50] with the aim of computing the mutual information between input and output trajectories [51]; in contrast to existing approaches [51], our PWS technique makes it possible to compute the mutual information between time-varying inputs and outputs exactly for this broad model class. In addition, we can generalize PWS to systems with feedback from the output to the input as shown in Appendix C.

In Section V we apply PWS to two well-known model systems. The first is a simple pair of coupled birth-death processes which allows us to test the efficiency of the three PWS variants, as well as to compare the PWS results with analytical results from the Gaussian approximation [6] and the technique by Duso and Zechner [30]. Our second example is a realistic model of the bacterial chemotaxis system, which is arguably the best characterized signaling system in biology. It has recently been argued that chemotaxis is information limited [52], a claim which requires an accurate evaluation of the mutual information. However, the chemotaxis system is a complex network consisting of 173 reactions, and the information transmission rate or multi-step transfer entropy cannot be obtained exactly with any previous technique. We not only show that PWS is capable of computing the mutual information between trajectories and hence the information rate, but also that this measure, unlike other information measures like the instantaneous mutual information, can reveal a generic principle for fast information transmission: the temporal dynamics of the input signal and the information-processing system must be matched.

## II. MONTE CARLO ESTIMATE OF THE MUTUAL INFORMATION

In this section we present the fundamental ideas that make up the PWS scheme. Specifically, we derive the Direct PWS algorithm as a simple yet exact scheme to compute the mutual information between trajectories. The DPWS algorithm is also the foundation of the other two more advanced PWS variants which will be explained in subsequent sections.

### A. Statement of the Problem

All information processing systems can be thought of as devices that repeatedly take an input value  $s$  and produce a corresponding output  $x$ . Crucially, due to the presence of noise, the output produced for the same input can be different every time, such that the system is sampling outputs from the distribution  $P(x|s)$ . In the information theoretic sense, the device's capabilities are fully specified by its output distributions for all possible inputs. We consider the inputs as being distributed according to a probability density  $P(s)$  such that the whole setup of signal and device is completely described by the

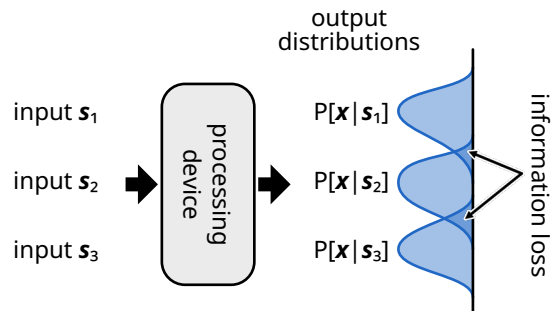


FIG. 1. Schematic of information processing under the influence of noise. Overlapping output distributions for different inputs lead to information loss since for any output in the overlapping region, we lose certainty over which input was fed into the device. The mutual information  $I(\mathcal{S}, \mathcal{X})$  quantifies how much information the observation of the output typically retains about the input signal.

joint probability density  $P(s, x) = P(s)P(x|s)$ .

In such a setup, because of noise, the output generally cannot accurately represent the input, i.e. information about the input can be lost. Loss of information happens when the output distributions of the device to different signals overlap each other. In such a case, an output in the overlap cannot be uniquely mapped back to its input (see Fig. 1). The remaining information that the output carries about the signal on average is measured by the mutual information between input and output.

Mathematically, the mutual information between a random variable  $\mathcal{S}$ , representing the input, and a second random variable  $\mathcal{X}$ , representing the output, is defined as

$$I(\mathcal{S}, \mathcal{X}) = \iint ds dx P(s, x) \ln \frac{P(s, x)}{P(s)P(x)}, \quad (1)$$

where the marginal output distribution is given by  $P(x) = \int ds P(s, x)$ . The quantity  $I(\mathcal{S}, \mathcal{X})$  as defined above is a non-negative real number, giving the mutual information between  $\mathcal{S}$  and  $\mathcal{X}$  in nats. The integral in Eq. (1) runs over all possible realizations of the random variables  $\mathcal{S}$  and  $\mathcal{X}$ . Specifically, we will be interested in the case where  $\mathcal{S}$  and  $\mathcal{X}$  are trajectory-valued, i.e. where each realization of  $\mathcal{S}$  and  $\mathcal{X}$  is a stochastic trajectory and the integral becomes a path integral.

In general, the mutual information can be decomposed into two terms, a conditional entropy and a marginal entropy. Due to the symmetry of Eq. (1) with respect to exchange of  $\mathcal{S}$  and  $\mathcal{X}$  this decomposition can be written as

$$I(\mathcal{S}, \mathcal{X}) = H(\mathcal{S}) - H(\mathcal{S}|\mathcal{X}) = H(\mathcal{X}) - H(\mathcal{X}|\mathcal{S}). \quad (2)$$

The (marginal) input entropy  $H(\mathcal{S})$  represents the total uncertainty about the input, and the conditional input entropy  $H(\mathcal{S}|\mathcal{X})$  describes the remaining uncertainty of the input after having observed the output. Thus, the mutual information  $I(\mathcal{S}, \mathcal{X}) = H(\mathcal{S}) - H(\mathcal{S}|\mathcal{X})$  naturally

quantifies the reduction in uncertainty about the input through the observation of the output.

When analyzing data from experiments or simulations however, the mutual information is generally estimated via  $I(\mathcal{S}, \mathcal{X}) = H(\mathcal{X}) - H(\mathcal{X}|\mathcal{S})$ . This formulation interprets the mutual information as quantifying the difference between the overall output uncertainty, and the output uncertainty with known input. The output uncertainties are easier to compute since experimental data and simulations generally provide information about the distribution of outputs for a given input, rather than vice versa. Therefore, the experimentally and computationally accessible entropy terms are the marginal output entropy  $H(\mathcal{X})$  and the conditional output entropy  $H(\mathcal{X}|\mathcal{S})$  which mathematically are defined as

$$H(\mathcal{X}) = - \int dx P(x) \ln P(x) \quad (3)$$

$$H(\mathcal{X}|\mathcal{S}) = - \int ds P(s) \int dx P(x|s) \ln P(x|s). \quad (4)$$

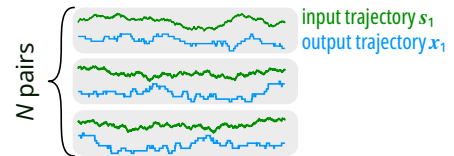
The conventional, model-free way of computing the mutual information using a stochastic simulation involves generating many samples, i.e. trajectories, to obtain empirical distribution estimates (e.g. histograms) for  $P(x|s)$  and  $P(x)$ . However, empirically estimating these probability distributions from measured or sampled data in a model-free fashion is difficult. Generally, the number of samples needs to be larger than the number of histogram bins to reduce the noise in the bin counts. This becomes particularly difficult, if not impossible, for high-dimensional output spaces, like signal trajectories. At the same time, any nonzero bin size leads to a systematic bias in the entropy estimates, already for one-dimensional entropy estimators [17]. This raises the question whether it is possible to compute the mutual information between trajectories without the need to estimate probability distributions using histograms.

## B. Direct PWS

Here, we present an exact Monte Carlo technique to compute the mutual information when the input  $\mathbf{s}$  and output  $\mathbf{x}$  are trajectories for the large class of systems described by a master equation. The scheme sidesteps the problem of estimating probability distributions in trajectory space via histograms by exploiting the idea that for these systems the output trajectory probability for a given input trajectory can be computed exactly. To emphasize that we are dealing with distributions of trajectories, we denote the conditional probability of producing a continuous-time output trajectory  $\mathbf{x}$  for a given input trajectory  $\mathbf{s}$  by  $\mathcal{P}[\mathbf{x}|\mathbf{s}]$ , and the probability to receive a specific input trajectory  $\mathbf{s}$  by  $\mathcal{P}[\mathbf{s}]$ . Specifically, we will show that

- for a system described by a master equation, the likelihood  $\mathcal{P}[\mathbf{x}|\mathbf{s}]$  is a quantity that can be computed on the fly in a stochastic simulation;

### 1. Simulate input output pairs $(x_i|s_i)$



### 2. Compute likelihoods $P[x_i|s_i]$

$$P[x|s] = P(x(t_0)) \prod_{i=1}^n P(x(t_{i-1}) \rightarrow x(t_i) | s)$$

### 3. Compute marginal probabilities $P[x_i]$

Direct PWS	RR-PWS	TI-PWS
Brute force estimate of the marginal probability $P[x]$ using direct samples from $P[s]$	Estimate of the marginal probability $P[x]$ using biased sampling, inspired by polymer simulations	MCMC estimate of the marginal probability $P[x]$ using thermodynamic integration

### 4. Compute the mutual information

$$I(\mathcal{S}, \mathcal{X}) = \frac{1}{N} \sum_{i=1}^N (\ln P[x_i|s_i] - \ln P[x_i])$$

FIG. 2. The PWS scheme to compute the mutual information between trajectories in 4 steps. **1.** Generate  $N$  input-output pairs from  $\mathcal{P}[\mathbf{s}, \mathbf{x}]$ . **2.** For each input-output pair compute the trajectory likelihood  $\mathcal{P}[\mathbf{x}_i|\mathbf{s}_i]$  using Eq. (15). **3.** Compute  $\mathcal{P}[\mathbf{x}_i]$  for every output. This step differentiates the different variants of PWS from each other. Direct PWS is presented in Section II B, whereas RR-PWS and TI-PWS are presented in Sections III B and III C. **4.** Using the likelihoods and the marginal probabilities from the previous steps we can estimate the mutual information using Eq. (10).

- input trajectories can be generated from  $\mathcal{P}[\mathbf{s}]$ , output trajectories for a given input  $\mathbf{s}$  can be generated according to  $\mathcal{P}[\mathbf{x}|\mathbf{s}]$  using standard SSA (Gillespie) simulations;
- by combining the two ideas above, we can derive a direct Monte Carlo estimate for the mutual information  $I(\mathcal{S}, \mathcal{X})$ .

Our technique is conceptually straightforward. Using Monte Carlo simulations we can compute averages over the configuration space of trajectories. Suppose we have a function  $f[\mathbf{z}]$  that takes a trajectory  $\mathbf{z}$  and produces a scalar value. We introduce notation for the average of  $f[\mathbf{z}]$  with respect to the trajectory distribution  $\mathcal{P}[\mathbf{z}]$ , which we write as

$$\langle f[\mathbf{z}] \rangle_{\mathcal{P}[\mathbf{z}]} \equiv \int \mathcal{D}[\mathbf{z}] \mathcal{P}[\mathbf{z}] f(\mathbf{z}). \quad (5)$$

We write  $\int \mathcal{D}[\mathbf{z}]$  to denote a path integral over all possible trajectories of a given duration. To estimate  $\langle f[\mathbf{z}] \rangle_{\mathcal{P}[\mathbf{z}]}$ , we can generate a large number of trajectories  $\mathbf{z}_1, \dots, \mathbf{z}_N$  from  $\mathcal{P}[\mathbf{z}]$  and evaluate the corresponding Monte Carlo average

$$\hat{f}_N = \frac{1}{N} \sum_{i=1}^N f(\mathbf{z}_i). \quad (6)$$

Specifically, we want to estimate the conditional and the marginal entropy as Monte Carlo averages to compute the mutual information. Let us imagine that we generate  $N$  input trajectories  $\mathbf{s}_1, \dots, \mathbf{s}_N$  from the distribution  $\mathcal{P}[\mathbf{s}]$ . Next, for every input  $\mathbf{s}_i$ , we generate a set of  $M$  outputs  $\mathbf{x}_{i,1}, \dots, \mathbf{x}_{i,M}$  from  $\mathcal{P}[\mathbf{x}|\mathbf{s}_i]$ . Then, the Monte Carlo estimate for the conditional entropy is

$$\begin{aligned} \mathrm{H}(\mathcal{X}|\mathcal{S}) &= - \int \mathcal{D}[\mathbf{s}] \mathcal{P}[\mathbf{s}] \int \mathcal{D}[\mathbf{x}] \mathcal{P}[\mathbf{x}|\mathbf{s}] \ln \mathcal{P}[\mathbf{x}|\mathbf{s}] \\ &= \left\langle \langle \ln \mathcal{P}[\mathbf{x}|\mathbf{s}] \rangle_{\mathcal{P}[\mathbf{x}|\mathbf{s}]} \right\rangle_{\mathcal{P}[\mathbf{s}]} \\ &\approx - \frac{1}{N} \sum_{i=1}^N \frac{1}{M} \sum_{j=1}^M \ln \mathcal{P}[\mathbf{x}_{i,j}|\mathbf{s}_i]. \end{aligned} \quad (7)$$

Secondly, if for a given output  $\mathbf{x}$  we generate  $K$  inputs  $\mathbf{s}'_1, \dots, \mathbf{s}'_K$  according to  $\mathcal{P}[\mathbf{s}]$ , then we can obtain a Monte Carlo estimate for the marginal probability of the output trajectory  $\mathcal{P}[\mathbf{x}]$ :

$$\begin{aligned} \mathcal{P}[\mathbf{x}] &= \int \mathcal{D}[\mathbf{s}] \mathcal{P}[\mathbf{s}] \mathcal{P}[\mathbf{x}|\mathbf{s}] \\ &= \langle \mathcal{P}[\mathbf{x}|\mathbf{s}] \rangle_{\mathcal{P}[\mathbf{s}]} \\ &\approx \frac{1}{K} \sum_{j=1}^K \mathcal{P}[\mathbf{x}|\mathbf{s}'_j]. \end{aligned} \quad (8)$$

The estimate for the marginal entropy is then given by

$$\begin{aligned} \mathrm{H}(\mathcal{X}) &= - \int \mathcal{D}[\mathbf{x}] \mathcal{P}[\mathbf{x}] \ln \mathcal{P}[\mathbf{x}] \\ &= - \langle \ln \mathcal{P}[\mathbf{x}] \rangle_{\mathcal{P}[\mathbf{x}]} \\ &\approx - \frac{1}{N} \sum_{i=1}^N \ln \mathcal{P}[\mathbf{x}_i] \\ &\approx - \frac{1}{N} \sum_{i=1}^N \ln \left[ \frac{1}{K} \sum_{j=1}^K \mathcal{P}[\mathbf{x}_i|\mathbf{s}'_{i,j}] \right]. \end{aligned} \quad (9)$$

In the last step we inserted the result from Eq. (8). In this estimate, the trajectories  $\mathbf{x}_1, \dots, \mathbf{x}_N$  are sampled from  $\mathcal{P}[\mathbf{x}]$  and for each  $\mathbf{x}_i$  we sample a set of input trajectories  $\mathbf{s}_{i,1}, \dots, \mathbf{s}_{i,K}$  from  $\mathcal{P}[\mathbf{s}]$ . Note that samples from  $\mathcal{P}[\mathbf{x}]$  are drawn by successively sampling from  $\mathcal{P}[\mathbf{s}]$  and  $\mathcal{P}[\mathbf{x}|\mathbf{s}]$ . Finally, the mutual information is computed by taking the difference of the entropies, i.e.  $\mathrm{I}(\mathcal{S}, \mathcal{X}) = \mathrm{H}(\mathcal{X}) - \mathrm{H}(\mathcal{X}|\mathcal{S})$ .

While this is the main idea behind the PWS technique, it is computationally advantageous to change the order of operations in the estimate. Specifically, computing the difference of two averages, i.e. computing the mutual information as a difference of entropies, leads to large statistical errors. We can obtain an improved estimate by reformulating the mutual information as a single average of differences:

$$\begin{aligned} \mathrm{I}(\mathcal{S}, \mathcal{X}) &= \int \mathcal{D}[\mathbf{s}] \int \mathcal{D}[\mathbf{x}] \mathcal{P}[\mathbf{s}, \mathbf{x}] \ln \frac{\mathcal{P}[\mathbf{x}|\mathbf{s}]}{\mathcal{P}[\mathbf{x}]} \\ &= \langle \ln \mathcal{P}[\mathbf{x}|\mathbf{s}] - \ln \mathcal{P}[\mathbf{x}] \rangle_{\mathcal{P}[\mathbf{s}, \mathbf{x}]} . \end{aligned} \quad (10)$$

Due to the reduction of variance when the estimate is performed this way, we base all PWS estimate on Eq. (10). The resulting PWS scheme is summarized in Fig. 2.

Note that to estimate Eq. (10) we still require two nested Monte Carlo averages since the marginal probability  $\mathcal{P}[\mathbf{x}]$  itself also needs to be computed by a Monte Carlo computation. In the brute-force version of PWS, called *Direct PWS* (DPWS), we use Eq. (8) to evaluate the marginal probability. In Section III below, we will present two additional variants of PWS where the brute-force estimate of the marginal probability  $\mathcal{P}[\mathbf{x}]$  is replaced by more elaborate schemes. That said, DPWS is a conceptually simple, straightforward to implement, and exact scheme to compute the mutual information.

To formulate a single equation summarizing the DPWS estimate of the mutual information we combine Eqs. (8) and (10). Using samples  $(\mathbf{s}_1, \mathbf{x}_1), \dots, (\mathbf{s}_N, \mathbf{x}_N)$  drawn from  $\mathcal{P}[\mathbf{s}, \mathbf{x}] = \mathcal{P}[\mathbf{s}] \mathcal{P}[\mathbf{x}|\mathbf{s}]$ , and additional input samples  $\mathbf{s}'_{i,j}$  drawn from  $\mathcal{P}[\mathbf{s}]$  for  $i = 1, \dots, N$  and  $j = 1, \dots, K$ , we compute

$$\hat{\mathrm{I}}(\mathcal{S}, \mathcal{X}) = \frac{1}{N} \sum_{i=1}^N \left[ \ln \mathcal{P}[\mathbf{x}_i|\mathbf{s}_i] - \ln \left( \sum_{j=1}^K \frac{\mathcal{P}[\mathbf{x}_i|\mathbf{s}'_{i,j}]}{K} \right) \right]. \quad (11)$$

The computational requirements for the evaluation of Eq. (11) are clear. Overall, we require  $N$  samples from the joint distribution  $\mathcal{P}[\mathbf{s}, \mathbf{x}]$  and  $NK$  additional samples from the input distribution  $\mathcal{P}[\mathbf{s}]$  for this estimate. These samples are obtained using standard SSA (Gillespie) simulations as shown below. Finally, to actually compute the Monte Carlo average, we have to evaluate the trajectory likelihood  $\mathcal{P}[\mathbf{x}|\mathbf{s}]$  a total of  $N(K+1)$  times.

We call the estimate in Eq. (11) *Direct PWS* since it is a direct Monte Carlo scheme to compute the mutual information. Specifically, not only is the mutual information computed as a direct Monte Carlo average over  $\ln \mathcal{P}[\mathbf{x}|\mathbf{s}] - \ln \mathcal{P}[\mathbf{x}]$  but also the marginal probability  $\mathcal{P}[\mathbf{x}]$  is computed via a nested direct Monte Carlo average.

Having explained the core ideas of our technique above, we will continue this section with a review of the necessary concepts of master equations to implement PWS. First, in Section II C, we derive the formula for the conditional probability  $\mathcal{P}[\mathbf{x}|\mathbf{s}]$  which lies at the heart of our technique. In Sections II C and II D, we discuss how trajectories are generated according to  $\mathcal{P}[\mathbf{x}|\mathbf{s}]$  and  $\mathcal{P}[\mathbf{s}]$ ,

which are the remaining ingredients required for using Direct PWS. Then, in Section III, we will present the two other variants of PWS that improve on Direct PWS.

### C. Driven Markov Jump Process

Throughout this article we consider systems that can be modeled by a master equation and are being driven by a stochastic input signal. The master equation describes a continuous time Markov process with a discrete state space  $\Omega$ . It specifies the time evolution of the conditional probability distribution  $P(x, t|x_0, t_0)$  which is the probability for the process to reach the state  $x \in \Omega$  at time  $t$ , given that it was at state  $x_0 \in \Omega$  at the previous time  $t_0$ . Note that the state space  $\Omega$  is multi-dimensional if the system is made up of multiple components and therefore  $x$  and  $x_0$  can be vectors rather than scalar values. We denote the transition rate at time  $t$  from state  $x$  to another state  $x' \neq x$  by  $w_t(x', x)$ . The master equation reads

$$\frac{\partial P(x, t)}{\partial t} = \sum_{\substack{x' \in \Omega \\ x' \neq x}} [w_t(x, x')P(x', t) - w_t(x', x)P(x, t)]. \quad (12)$$

For brevity, we suppress the dependence on the initial condition  $x_0, t_0$  in the notation, i.e.  $P(x, t) = P(x, t|x_0, t_0)$ .

By defining  $Q_t(x', x) = w_t(x', x)$  for  $x \neq x'$  and  $Q_t(x, x) = -\sum_{x' \in \Omega \setminus \{x\}} w_t(x', x)$  we can simplify the master equation to

$$\frac{\partial P(x, t)}{\partial t} = \sum_{x' \in \Omega} Q_t(x, x')P(x', t) \quad (13)$$

which formally resembles a matrix multiplication of  $Q_t$  and  $P(\cdot, t)$ . Note that by definition the diagonal matrix element  $Q_t(x, x)$  is the negative exit rate from state  $x$ , i.e. the total rate at which probability flows away from state  $x$ .

Using the master equation we can compute the probability of any trajectory of the corresponding jump process. A trajectory  $\mathbf{x}$  of a jump process is defined by a list of jump times  $t_1, \dots, t_{n-1}$ , together with a sequence of system states  $x_0, \dots, x_{n-1}$ . The trajectory starts at time  $t_0$  in state  $x_0$  and ends at time  $t_n$  in state  $x_{n-1}$ , and at each time  $t_i$  (for  $i = 1, \dots, n-1$ ) the trajectory describes an instantaneous jump  $x_{i-1} \rightarrow x_i$ . The duration of a trajectory is  $T = t_n - t_0$ . The standard expression for the probability density of a single trajectory  $\mathbf{x}$  is

$$\mathcal{P}[\mathbf{x}] = P(x_0) \times \left( \prod_{i=1}^{n-1} Q_{t_i}(x_i, x_{i-1}) \right) \times \left( \prod_{i=1}^n \exp \int_{t_{i-1}}^{t_i} dt Q_t(x_{i-1}, x_{i-1}) \right). \quad (14)$$

Thus, the trajectory probability is a product of the probability of the initial state  $P(x_0)$ , the rates of the  $n-1$  transitions  $Q_{t_i}(x_i, x_{i-1})$ , and the survival probabilities for the  $n$  waiting times  $t_i - t_{i-1}$  given by  $\exp \int_{t_{i-1}}^{t_i} dt Q_t(x_{i-1}, x_{i-1})$ .

#### 1. Computing the Likelihood $\mathcal{P}[\mathbf{x}|\mathbf{s}]$

In our setup, we assume the jump process is driven by a stochastic input trajectory  $\mathbf{s}$  and we want to compute the conditional probability  $\mathcal{P}[\mathbf{x}|\mathbf{s}]$  of an output trajectory  $\mathbf{x}$ . This quantity is the *likelihood* of the observation  $\mathbf{x}$  for the given input  $\mathbf{s}$ . In a driven system, the input trajectory determines the time-dependent stochastic dynamics of the jump process, i.e. the transition rates at time  $t$ , given by  $Q_t(x', x)$ , depend explicitly on the input  $s(t)$  at time  $t$ . Thus, for any given input trajectory  $\mathbf{s}$ , the jump process produces trajectories according to the transition rate matrix  $Q_t(x', x; \mathbf{s})$  which denotes the time-dependent transition rates induced by the given input trajectory. Generally, the transition rates at time  $t$ , given by  $Q_t(x', x; \mathbf{s})$ , may depend on the entire history of  $\mathbf{s}$  prior to  $t$ .

The corresponding probability distribution of generated output trajectories is characterized by the density  $\mathcal{P}[\mathbf{x}|\mathbf{s}]$ , i.e. each input trajectory produces a different ensemble of output trajectories. In the common case that every input trajectory  $\mathbf{s}$  leads to a unique transition rate matrix  $Q_t(x', x; \mathbf{s})$ , i.e. the map  $\mathbf{s} \mapsto Q_t(\cdot, \cdot; \mathbf{s})$  is injective, the likelihood is directly given by Eq. (14):

$$\mathcal{P}[\mathbf{x}|\mathbf{s}] = P(x_0|s_0) \times \left( \prod_{i=1}^{n-1} Q_{t_i}(x_i, x_{i-1}; \mathbf{s}) \right) \times \left( \prod_{i=1}^n \exp \int_{t_{i-1}}^{t_i} dt Q_t(x_{i-1}, x_{i-1}; \mathbf{s}) \right) \quad (15)$$

where  $P(x_0|s_0)$  is the probability of the initial state  $x_0$  at  $t_0$  given the corresponding value of the input trajectory  $s_0 = s(t_0)$ .

The evaluation of the trajectory likelihood is at the heart of our Monte Carlo scheme. However, numerically computing a large product like Eq. (15) very quickly reaches the limits of floating point arithmetic since the result is often either too large or too close to zero to be representable as a floating point number. Thus, to avoid numerical issues, it is vital to perform the computations in log-space, i.e. to compute

$$\ln \mathcal{P}[\mathbf{x}|\mathbf{s}] = \ln P(x_0|s_0) + \int_{t_0}^T dt \mathcal{L}_t[\mathbf{s}, \mathbf{x}] \quad (16)$$

where

$$\mathcal{L}_t[\mathbf{s}, \mathbf{x}] = Q_t(x(t), x(t); \mathbf{s}) + \sum_{i=1}^{n-1} \delta(t - t_i) \ln Q_t(x_i, x_{i-1}; \mathbf{s}). \quad (17)$$

The computation of the log-likelihood  $\ln \mathcal{P}[\mathbf{x}|\mathbf{s}]$  for given trajectories  $\mathbf{s}$  and  $\mathbf{x}$  according to Eqs. (16) and (17) proceeds analogous to a Gillespie simulation of the corresponding master equation for  $\mathbf{x}$  conditioned on  $\mathbf{s}$ . During the evaluation of the log-likelihood we effectively “retrace” the trajectory of  $\mathbf{x}$  and accumulate the log probability as follows:

- At the start of the trajectory we add the log-probability of the initial condition  $\ln P(x_0|s_0)$ ,
- for every jump  $x_{i-1} \rightarrow x_i$  in  $\mathbf{x}$  we add the log jump propensity  $\ln Q_{t_i}(x_i, x_{i-1}; \mathbf{s})$  to the accumulated value, and
- for every interval  $(t_{i-1}, t_i)$  of constant output value  $x(t) = x_{i-1}$  between two jumps of  $\mathbf{x}$  we add a contribution of  $\int_{t_{i-1}}^{t_i} dt Q_t(x_{i-1}, x_{i-1}; \mathbf{s})$  to the accumulated value. This integral can be performed using standard numerical methods such as the trapezoidal rule, which is also exact if  $Q_t(x(t), x(t); \mathbf{s})$  is a piecewise linear function of  $t$  as in our examples in Section V.

The sum of the three contributions above yields the exact log-likelihood  $\ln \mathcal{P}[\mathbf{x}|\mathbf{s}]$  as given in Eq. (16).

Thus, notably, the algorithm to compute the log-likelihood  $\ln \mathcal{P}[\mathbf{x}|\mathbf{s}]$  is both efficient and straightforward to implement, being closely related to the standard Gillespie algorithm. The only quantity in Eq. (16) that cannot be directly obtained from the master equation is the log-probability of the initial state,  $\ln P(x_0|s_0)$ .

Indeed,  $P(x_0|s_0)$  does not only depend on the stochastic dynamics as specified by the master equation, but on the separately specified initial condition of the system. The initial condition is defined by the distribution  $P(s_0, x_0)$  which is the distribution of initial points of the  $\mathbf{s}$  and  $\mathbf{x}$  trajectories. While our scheme can be applied to any system with a well-defined (non-equilibrium) initial distribution  $P(s_0, x_0)$  as specified by, e.g. the experimental setup, in many cases we are interested in studying information transmission for systems in steady state. Then, the initial condition is given by the stationary distribution of the Markov process which can, depending on the complexity of the system, either be computed analytically from the master equation [53, 54] (possibly using simplifying approximations [55, 56]), or computationally using stochastic simulations [57].

## 2. Sampling from $\mathcal{P}[\mathbf{x}|\mathbf{s}]$

Standard kinetic Monte Carlo simulations naturally produce exact samples of the probability distribution with the density  $\mathcal{P}[\mathbf{x}|\mathbf{s}]$  as defined in Eq. (15). That is, for any signal trajectory  $\mathbf{s}$  and initial state  $x_0$  drawn from  $P(x_0|s_0)$  we can use the Stochastic Simulation Algorithm (SSA) or variants thereof to generate a corresponding trajectory  $\mathbf{x}$ . The SSA exactly propagates the initial

condition  $x_0, t_0$  forward in time according to the transition rate matrix  $Q_t(\cdot; \mathbf{s})$ . In the standard Direct SSA algorithm [57] this is done by alternately sampling the waiting time until the next transition, and then selecting the actual transition.

Note that the transition rates  $Q_t(x', x; \mathbf{s})$  of a driven master equation are necessarily time-dependent since they include the coupling of the jump process to the input trajectory  $\mathbf{s}$ , which itself varies in time. While standard descriptions of the SSA often assume that the transition rates are constant, this restriction is easily lifted. Specifically, for the commonly used Direct SSA algorithm the main issue with non-constant transition rates presents itself in the sampling of the stochastic waiting times. Consider step  $i$  of the algorithm which generates the next transition time  $t_{i+1} = t_i + \Delta t_i$ . For time-varying transition rates the distribution of the stochastic waiting time  $\Delta t_i$  is characterized by the survival function

$$S_i(\tau) = P(\Delta t_i > \tau) = \exp \int_{t_i}^{t_i + \tau} dt Q_t(x_i, x_i; \mathbf{s}). \quad (18)$$

Sampling the waiting time can be achieved using inverse transform sampling, i.e. by generating a uniformly distributed random number  $u \in [0, 1]$  and computing the waiting time using the inverse survival function  $\Delta t_i = S_i^{-1}(u)$ . Numerically, computing the inverse of the survival function requires solving the equation

$$\ln u = \int_{t_i}^{t_i + \Delta t_i} dt Q_t(x_i, x_i; \mathbf{s}) \quad (19)$$

for the waiting time  $\Delta t_i$ . Depending on the complexity of the expression for  $Q_t(x_i, x_i; \mathbf{s})$ , this equation can either be solved analytically or numerically, e.g. using Newton’s method. Hence, this method to generate stochastic trajectories is only truly *exact* if we can solve Eq. (19) analytically, as in the examples from Section V. Additionally, we want to point out that in some cases more efficient variants of the SSA with time dependent rates could be used [58, 59].

## D. Input Statistics

For our mutual information estimate, we need to be able to draw samples from the input trajectory distribution given by  $\mathcal{P}[\mathbf{s}]$ . Indeed, our simulation algorithm poses no restrictions for the choice of input signal distribution  $\mathcal{P}[\mathbf{s}]$  other than the possibility to generate sample input trajectories. For instance, if the input signal is itself described by a continuous-time jump process, we can generate trajectories using the SSA. Indeed, the two examples studied in Section V both use input signals that are described by a chemical master equation.

One benefit of using input trajectories generated by a stochastic jump process is that it is possible to generate exact realizations of such a process (using the SSA) and to exactly compute the likelihood  $\mathcal{P}[\mathbf{x}|\mathbf{s}]$  using Eq. (16).

Specifically, the likelihood can be exactly evaluated because the transition rates  $Q_t(\cdot, \cdot; \mathbf{s})$  for any input trajectory  $\mathbf{s}$ , while time-dependent, are *piece-wise constant*. This implies that the integral in Eq. (16) can be evaluated analytically without approximations. Similarly, for piece-wise constant transition rates, the inverse function of Eq. (19) can be evaluated directly such that we can sample exact trajectories from the driven jump process. As a result, when both input and output are described by a master equation, PWS is a completely exact Monte Carlo scheme to compute the mutual information.

However, the techniques described here do *not* require the input signal  $\mathbf{s}$  to be described by a continuous-time jump process, or, indeed, to be Markovian. The input signal can be any stochastic process for which trajectories can be generated numerically. This includes continuous stochastic processes that are found as solutions to stochastic differential equations, for which many algorithms exist to generate trajectories [60].

### III. VARIANTS OF PWS

The Direct PWS simulation scheme presented in the previous section makes it possible to compute the mutual information between trajectories of a stochastic input process and the output of a Markov jump process. Yet, due to the combinatorial explosion of possible trajectories, the variance of the DPWS estimate increases exponentially with trajectory length. Hence, for complex information processing networks and long trajectories the direct PWS estimate may incur very high computational cost. In this section we rephrase the computation of the mutual information in terms of free-energy calculations. Based on this formulation of the problem we present two improved variants of PWS whose computational efficiency allows us to study more complex information processing networks.

#### A. Marginalization Integrals in Trajectory Space

The computationally most demanding part of our scheme in Section II B is the evaluation of the marginalization integral  $\mathcal{P}[\mathbf{x}] = \int \mathcal{D}[\mathbf{s}] \mathcal{P}[\mathbf{s}, \mathbf{x}]$  which needs to be computed repeatedly for many different responses  $\mathbf{x}_1, \dots, \mathbf{x}_N$  in our PWS scheme. Consequently the computational efficiency of the marginalization is essential for the overall simulation performance.

Marginalization is a general term to denote an operation where one or more variables are integrated out of a joint probability distribution, say  $\mathcal{P}[\mathbf{s}, \mathbf{x}]$ , to obtain the corresponding marginal probability distribution  $\mathcal{P}[\mathbf{x}]$ :

$$\mathcal{P}[\mathbf{x}] = \int \mathcal{D}[\mathbf{s}] \mathcal{P}[\mathbf{s}, \mathbf{x}]. \quad (20)$$

In DPWS, we use the estimate in Eq. (8) to compute  $\mathcal{P}[\mathbf{x}]$  which involves generating input trajectories from

$\mathcal{P}[\mathbf{s}]$ . However, this is not the optimal Monte Carlo sampling distribution since the generated input trajectories are independent from the output trajectory  $\mathbf{x}$ , i.e. we ignore the causal connection between  $\mathbf{s}$  and  $\mathbf{x}$ . Consequently, we could frequently end up sampling a trajectory  $\mathbf{s}^*$  with a likelihood  $\mathcal{P}[\mathbf{x}|\mathbf{s}^*]$  that is very small. Hence, only a very small number of samples might contribute significantly to the average, and the variance of the result could well be much larger than the overall sample size  $M$  would suggest. Thus, the use of  $\mathcal{P}[\mathbf{s}]$  as the sampling distribution is only practical in cases where the dependence of the output on the input is not too strong, or in other words, when, perhaps paradoxically, the mutual information is not too large [61].

This is a well known Monte Carlo sampling problem and a large number of techniques have been developed to solve it. Especially in computational statistical physics, similar sampling issues are frequently encountered in the computation of free energies, and thus the two improved variants of our scheme, RR-PWS and TI-PWS, both make use of ideas originating from statistical physics.

To understand how we can make use of these ideas to compute the marginal probability  $\mathcal{P}[\mathbf{x}]$ , it is convenient to rephrase the marginalization integral in Eq. (20) in the language of statistical physics. In this language,  $\mathcal{P}[\mathbf{x}]$  corresponds to the normalization constant, or partition function, of a Boltzmann distribution for the potential

$$\mathcal{U}[\mathbf{s}, \mathbf{x}] = -\ln \mathcal{P}[\mathbf{s}, \mathbf{x}]. \quad (21)$$

In Eq. (21), we interpret  $\mathbf{s}$  as a variable in the configuration space whereas  $\mathbf{x}$  is an auxiliary variable, i.e. a parameter. Note that both  $\mathbf{s}$  and  $\mathbf{x}$  still represent trajectories. For this potential, the partition function is given by

$$\mathcal{Z}[\mathbf{x}] = \int \mathcal{D}[\mathbf{s}] e^{-\mathcal{U}[\mathbf{s}, \mathbf{x}]}. \quad (22)$$

The integral only runs over the configuration space, i.e. we integrate only with respect to  $\mathbf{s}$  but not  $\mathbf{x}$ , which remains a parameter of the partition function. The partition function is precisely equal to the marginal probability of the output, i.e.  $\mathcal{Z}[\mathbf{x}] = \mathcal{P}[\mathbf{x}]$ , as can be verified

$\mathcal{P}[\mathbf{s}, \mathbf{x}]$	$e^{-\mathcal{U}[\mathbf{s}, \mathbf{x}]}$
$\mathcal{P}[\mathbf{s}]$	$\frac{1}{\mathcal{Z}_0[\mathbf{x}]} e^{-\mathcal{U}_0[\mathbf{s}]}$
$\mathcal{P}[\mathbf{s} \mathbf{x}]$	$\frac{1}{\mathcal{Z}[\mathbf{x}]} e^{-\mathcal{U}[\mathbf{s}, \mathbf{x}]}$
1	$\mathcal{Z}_0[\mathbf{x}]$
$\mathcal{P}[\mathbf{x}]$	$\mathcal{Z}[\mathbf{x}]$
$\mathcal{P}[\mathbf{x} \mathbf{s}]$	$e^{-\Delta\mathcal{U}[\mathbf{s}, \mathbf{x}]}$

TABLE I. Translation to the notation of statistical physics. The definitions of  $\mathcal{U}$  and  $\mathcal{U}_0$  that are used here are given in Eqs. (21) and (25).



by inserting the expression for the  $\mathcal{U}[\mathbf{s}, \mathbf{x}]$ . Further, the free energy is given by

$$\mathcal{F}[\mathbf{x}] = -\ln \mathcal{Z}[\mathbf{x}] = -\ln \mathcal{P}[\mathbf{x}] \quad (23)$$

which shows that the computation of the free energy of the trajectory ensemble corresponding to  $\mathcal{U}[\mathbf{s}, \mathbf{x}]$  is equivalent to the computation of (the logarithm of) the marginal probability  $\mathcal{P}[\mathbf{x}]$ .

Note that above we omitted any factors of  $k_B T$  since temperature is irrelevant here. Also note that while the distribution  $\exp(-\mathcal{U}[\mathbf{s}, \mathbf{x}])$  looks like the equilibrium distribution of a canonical ensemble from statistical mechanics, this does not imply that we can only study systems in thermal equilibrium. Indeed, PWS is used to study information transmission in systems driven out of equilibrium by the input signal. Thus, the notation introduced in this section is nothing else but a mathematical reformulation of the marginalization integral to make the analogy to statistical physics apparent and we assign no additional meaning of the potentials and free energies introduced here.

In statistical physics it is well known that the free energy cannot be directly measured from a simulation. Instead, one estimates the free-energy difference

$$\Delta\mathcal{F}[\mathbf{x}] = \mathcal{F}[\mathbf{x}] - \mathcal{F}_0[\mathbf{x}] = -\ln \frac{\mathcal{Z}[\mathbf{x}]}{\mathcal{Z}_0[\mathbf{x}]} \quad (24)$$

between the system and a reference system with known free energy  $\mathcal{F}_0[\mathbf{x}]$ . The reference system is described by the potential  $\mathcal{U}_0[\mathbf{s}, \mathbf{x}]$  with the corresponding partition function  $\mathcal{Z}_0[\mathbf{x}]$ . In our case, a natural choice of reference potential is

$$\mathcal{U}_0[\mathbf{s}, \mathbf{x}] = -\ln \mathcal{P}[\mathbf{s}] \quad (25)$$

with the corresponding partition function

$$\mathcal{Z}_0[\mathbf{x}] = \int \mathcal{D}[\mathbf{s}] \mathcal{P}[\mathbf{s}] = 1. \quad (26)$$

This means that since  $\mathcal{P}[\mathbf{s}]$  is a normalized probability density function, the reference free energy is zero ( $\mathcal{F}_0[\mathbf{x}] = -\ln \mathcal{Z}_0[\mathbf{x}] = 0$ ). Hence, for the above choice of reference system, the free-energy difference is

$$\Delta\mathcal{F}[\mathbf{x}] = \mathcal{F}[\mathbf{x}] = -\ln \mathcal{P}[\mathbf{x}]. \quad (27)$$

Note that in our case the reference potential  $\mathcal{U}_0[\mathbf{s}, \mathbf{x}] = -\ln \mathcal{P}[\mathbf{s}]$  does not depend on the output trajectory  $\mathbf{x}$ , i.e.  $\mathcal{U}_0[\mathbf{s}, \mathbf{x}] \equiv \mathcal{U}_0[\mathbf{s}]$ . It describes a *non-interacting* version of our input-output system where the input trajectories evolve completely independently of the fixed output trajectory  $\mathbf{x}$ .

What is the interaction between the output  $\mathbf{x}$  and the input trajectory ensemble? We define the interaction potential  $\Delta\mathcal{U}[\mathbf{s}, \mathbf{x}]$  through

$$\mathcal{U}[\mathbf{s}, \mathbf{x}] = \mathcal{U}_0[\mathbf{s}] + \Delta\mathcal{U}[\mathbf{s}, \mathbf{x}]. \quad (28)$$

The interaction potential makes it apparent that the distribution of  $\mathbf{s}$  trajectories corresponding to the potential  $\mathcal{U}[\mathbf{s}, \mathbf{x}]$  is biased by  $\mathbf{x}$  with respect to the distribution corresponding to the reference potential  $\mathcal{U}_0[\mathbf{s}]$ . By inserting the expressions for  $\mathcal{U}_0[\mathbf{s}]$  and  $\mathcal{U}[\mathbf{s}, \mathbf{x}]$  into Eq. (28) we see that

$$\begin{aligned} \Delta\mathcal{U}[\mathbf{s}, \mathbf{x}] &= -\ln \mathcal{P}[\mathbf{x}|\mathbf{s}] \\ &= -\ln \mathcal{P}(x_0|s_0) - \int_0^T dt \mathcal{L}_t[\mathbf{s}, \mathbf{x}] \end{aligned} \quad (29)$$

where the second line is expressed using  $\mathcal{L}_t[\mathbf{s}, \mathbf{x}]$  from Eq. (16). This expression illustrates that the interaction of the output trajectory  $\mathbf{x}$  with the ensemble of input trajectories is characterized by the trajectory likelihood  $\mathcal{P}[\mathbf{x}|\mathbf{s}]$ . Since we can compute the trajectory likelihood from the master equation, so can we compute the interaction potential.

In this section we have introduced notation (summarized in Table I) to show that computing a marginalization integral is equivalent to the computation of a free-energy difference. This picture allows us to distinguish two input trajectory ensembles, the *non-interacting* ensemble distributed according to  $\exp(-\mathcal{U}_0[\mathbf{s}]) = \mathcal{P}[\mathbf{s}]$ , and the *interacting* ensemble with input distribution proportional to  $\exp(-\mathcal{U}[\mathbf{s}, \mathbf{x}]) \propto \mathcal{P}[\mathbf{s}|\mathbf{x}]$ . For example, the brute force estimate of  $\mathcal{P}[\mathbf{x}]$  used in DPWS can be written as

$$\mathcal{P}[\mathbf{x}] = \frac{\mathcal{Z}[\mathbf{x}]}{\mathcal{Z}_0[\mathbf{x}]} = \langle e^{-\Delta\mathcal{U}[\mathbf{s}, \mathbf{x}]} \rangle_0 \quad (30)$$

where the notation  $\langle \dots \rangle_0$  refers to an average with respect to the non-interacting ensemble. By inserting the expressions for  $\mathcal{U}_0$  and  $\Delta\mathcal{U}$ , it is easy to verify that this estimate is equivalent to Eq. (8). As explained in Section II B, to compute Eq. (30) using a Monte Carlo estimate, it is only necessary to sample from the non-interacting system  $\mathcal{U}_0[\mathbf{s}]$  and to compute the Boltzmann weight  $\Delta\mathcal{U}[\mathbf{s}, \mathbf{x}]$  (i.e. to sample from  $\mathcal{P}[\mathbf{s}]$  and to compute the log-likelihood  $\ln \mathcal{P}[\mathbf{x}|\mathbf{s}]$ ). This is indeed the DPWS scheme. However, by noting the correspondence between signal trajectories and polymers and that Eq. (24) has the same form as the expression for the (excess) chemical potential of a polymer, which is the free-energy difference between the polymer of interest and the ideal chain [42, 62], more efficient schemes can be developed, as we show next.

## B. RR-PWS

In Rosenbluth-Rosenbluth PWS we compute the free-energy difference  $\Delta\mathcal{F}$  between the ideal system  $\mathcal{U}_0$  and  $\mathcal{U}$  in a *single* simulation just like in the brute force method. However, instead of generating  $\mathbf{s}$  trajectories in an uncorrelated fashion according to  $\exp(-\mathcal{U}_0[\mathbf{s}]) = \mathcal{P}[\mathbf{s}]$ , we bias our sampling distribution towards  $\exp(-\mathcal{U}[\mathbf{s}, \mathbf{x}]) \propto \mathcal{P}[\mathbf{s}|\mathbf{x}]$  to reduce the sampling problems found in DPWS.

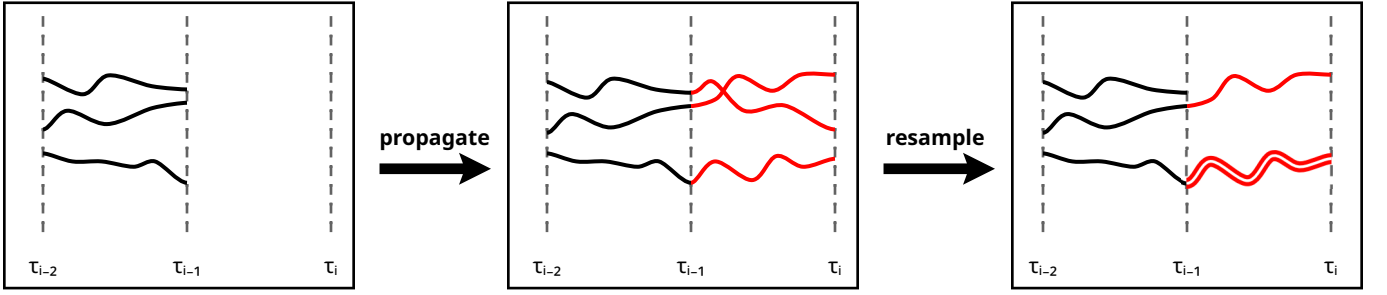


FIG. 3. Illustration of one step of the bootstrap particle filter in RR-PWS. We start with a set of trajectories  $\mathbf{s}_{[0, i-1]}^k$  with time span  $[\tau_0, \tau_{i-1}]$  (left panel). In the next step we propagate these trajectories forward in time to  $\tau_i$ , according to  $\mathcal{P}[\mathbf{s}]$  (central panel). Then we resample the trajectories according to the Boltzmann weights of their most recent segments, effectively eliminating or duplicating individual segments. An example outcome of the resampling step is shown in the right panel where the bottom trajectory was duplicated and one of the top trajectories was eliminated. These steps are repeated for each segment, until a set of input trajectories of the desired length is generated. The intermediate resampling steps bias the trajectory distribution from  $\mathcal{P}[\mathbf{s}]$  towards  $\mathcal{P}[\mathbf{s}|\mathbf{x}]$ .

The classical scheme for biasing the sampling distribution in polymer physics is due to Rosenbluth and Rosenbluth [63] in their study of self-avoiding chains. A substantial improvement of the Rosenbluth algorithm was achieved by Grassberger, by generating polymers using pruning and enrichment steps, thereby eliminating configurations that do not significantly contribute to the average. This scheme is known as the pruned-enriched Rosenbluth method, or PERM [43]. While PERM is much more powerful than the standard Rosenbluth algorithm, its main drawback is that it requires careful tuning of the pruning and enrichment schedule to achieve optimal convergence. Therefore we have opted to use a technique that is similar in spirit to PERM but requires less tuning, the bootstrap particle filter [64]. We will describe how to use PWS with a particle filter below. That said, we want to stress that the particle filter can easily be replaced by PERM or other related methods [65]. Also schemes inspired by variants of Forward Flux Sampling [66, 67] could be developed.

In the methods discussed above, a polymer is grown monomer by monomer. In a continuous-time Markov process this translates to trajectories being grown segment by segment. To define the segments, we introduce a time discretization  $0 < \tau_1 < \tau_2 < \dots < \tau_{n-1} < T$ . Thus, each trajectory  $\mathbf{s}$  of duration  $T$  consists of  $n$  segments where we denote the segment between  $\tau_i$  and  $\tau_j$  by  $\mathbf{s}_{[i, j]}$  (we define  $\tau_0 = 0$  and  $\tau_n = T$ ). The particle filter uses the following procedure to grow an ensemble of trajectories segment by segment:

1. Generate  $M$  starting points  $s_0^1, \dots, s_0^M$  according to the initial condition of the input signal  $P(s_0)$ .
2. Iterate for  $i = 1, \dots, n$ :
  - (a) Starting with an ensemble of  $M$  partial trajectories of duration  $\tau_{i-1}$  (if  $i = 1$  an ensemble of starting points) which we label  $\mathbf{s}_{[0, i-1]}^k$  for

$k = 1, \dots, M$ :

$$\left( \mathbf{s}_{[0, i-1]}^1, \dots, \mathbf{s}_{[0, i-1]}^M \right), \quad (31)$$

propagate each trajectory (or each starting point) forward in time from  $\tau_{i-1}$  to  $\tau_i$ . Propagation is performed according to the natural dynamics of  $\mathbf{s}$ , i.e. generating a new segment  $\mathbf{s}_{[i-1, i]}^k$  with probability

$$p_i^{\text{gen}}(k) = \mathcal{P} \left[ \mathbf{s}_{[i-1, i]}^k | \mathbf{s}_{[0, i-1]}^k \right] = e^{-\mathcal{U}_0[\mathbf{s}_{[i-1, i]}^k]} \quad (32)$$

for  $k = 1, \dots, M$ .

- (b) Compute the Boltzmann weight

$$U_i^k = \Delta \mathcal{U}[\mathbf{s}_{[i-1, i]}^k, \mathbf{x}_{[i-1, i]}] \quad (33)$$

of each new segment. This Boltzmann weight of a segment from  $\tau_{i-1}$  to  $\tau_i$  can be expressed as

$$U_i^k = -\delta_{1i} \ln P(x_0 | s_0) - \int_{\tau_{i-1}}^{\tau_i} dt \mathcal{L}_t[\mathbf{s}_{[i-1, i]}^k, \mathbf{x}_{[i-1, i]}], \quad (34)$$

see Eq. (29), and is therefore straightforward to compute from the master equation.

- (c) Sample  $M$  times from the distribution

$$p_i^{\text{select}}(k) = \frac{e^{-U_i^k}}{w_i} \quad (35)$$

where the Rosenbluth weight  $w_i$  is defined as

$$w_i = \sum_{k=1}^M e^{-U_i^k}. \quad (36)$$

This sampling procedure yields  $M$  randomly drawn indices  $\ell_i^1, \dots, \ell_i^M$ . Each  $\ell_i^k$  lies in the range from  $1, \dots, M$  and refers to one of the

trajectories in the ensemble,  $\mathbf{s}_{[0,i]}^{\ell_i^k}$ . We define the resampled set of trajectories by  $\tilde{\mathbf{s}}_{[0,i]}^k \equiv \mathbf{s}_{[0,i]}^{\ell_i^k}$  for  $k = 1, \dots, M$ . In this sense, the index  $\ell_i^k$  denotes the ancestor of  $\tilde{\mathbf{s}}_{[0,i]}^k$ . The list  $(\tilde{\mathbf{s}}_{[0,i]}^1, \dots, \tilde{\mathbf{s}}_{[0,i]}^M)$  is subsequently used as the input for the next iteration of the algorithm.

The normalized Rosenbluth factor of the final ensemble is then given by

$$\mathcal{W} = \prod_{i=1}^n \frac{w_i}{M}. \quad (37)$$

As shown in Appendix A, we can derive an *unbiased* estimate for the desired ratio  $\mathcal{Z}[\mathbf{x}]/\mathcal{Z}_0[\mathbf{x}] = \mathcal{P}[\mathbf{x}]$  based on the Rosenbluth factor:

$$\hat{\mathcal{P}}[\mathbf{x}] = \mathcal{P}(x_0) \mathcal{W} \quad (38)$$

with  $\mathcal{P}(x_0)$  being the probability of the initial output  $x_0$ . The particle filter can therefore be integrated into the DPWS algorithm to compute the marginal density  $\mathcal{P}[\mathbf{x}]$ , substituting the brute-force estimate given in Eq. (8). We call the resulting algorithm to compute the mutual information *RR-PWS*.

We now provide an intuitive explanation for the scheme presented above. First note that steps 1 and 2(a) of the procedure above involve just propagating  $M$  trajectories in parallel, according to  $\mathcal{P}[\mathbf{s}] = \exp(-\mathcal{U}_0[\mathbf{s}])$ . The interesting steps are 2(b-c) where we eliminate or duplicate some of the trajectories according to the Boltzmann weights of the most recent segment. Note, that in general the list of indices  $(\ell_i^1, \dots, \ell_i^M)$  that are sampled in step 2(c) will contain duplicates ( $\ell_i^k = \ell_i^{k'}$  for  $k \neq k'$ ), thus cloning the corresponding trajectory. Concomitantly, the indices  $\ell_i^1, \dots, \ell_i^M$  may not include every original index  $1, \dots, M$ , therefore eliminating some trajectories. Since indices of trajectories with high Boltzmann weight are more likely to be sampled from Eq. (35), this ensures that we are only spending computational effort on propagating those trajectories whose Boltzmann weight is not too small. Hence, at its heart the particle filter is an algorithm for producing samples that tend to be distributed according to  $\exp(-\mathcal{U}_0[\mathbf{s}]) \exp(-\Delta\mathcal{U}[\mathbf{s}, \mathbf{x}]) = \exp(-\mathcal{U}[\mathbf{s}, \mathbf{x}])$ , i.e. according to the Boltzmann distribution of the *interacting* ensemble, see also Appendix A. For illustration of the algorithm, one iteration of the particle filter is presented schematically in Fig. 3.

For the efficiency of the particle filter it is important to correctly choose the number of segments  $n$  which controls how often we resample within the trajectory ensemble. Since each resampling step introduces variance into the estimate, we want to resample as infrequently as possible. Yet, the longer the segments become, the wider will the distribution of Boltzmann weights  $U_i^k$  for a given segment  $i$  be, which means that only few of these weights contribute substantially to the corresponding Rosenbluth

weight  $w_i$ . To avoid both of these issues, we use an adaptive resampling schedule based on the effective sample size (ESS)

$$M_i^{(\text{eff})} = \frac{w_i^2}{\sum_{k=1}^M (e^{-U_i^k})^2} \quad (39)$$

of the Boltzmann weights as described in Ref. [68]: as a rule of thumb, we resample only when the  $M_i^{(\text{eff})}$  drops below  $M/2$ . Additionally, as recommended in Ref. [69], we use the *systematic sampling* algorithm to randomly draw the indices in step 2(c) to reduce the variance introduced at each resampling step. Using these techniques, the only parameter that needs to be chosen by hand for the particle filter is the ensemble size  $M$ .

### C. TI-PWS

Our third scheme, thermodynamic integration PWS (TI-PWS), is based on the analogy of marginalization integrals with free energy computations. As before, we view the problem of computing the marginal probability  $\mathcal{P}[\mathbf{x}]$  as equivalent to that of computing the free energy between ensembles that are defined by the potentials  $\mathcal{U}_0[\mathbf{s}, \mathbf{x}]$  and  $\mathcal{U}[\mathbf{s}, \mathbf{x}]$ , respectively. For the TI-PWS estimate we additionally assume that there is a continuous parameter that transforms the ensemble from  $\mathcal{U}_0$  to  $\mathcal{U}$ . Mathematically, we thus have a continuous mapping from  $\theta \in [0, 1]$  to a potential  $\mathcal{U}_\theta[\mathbf{s}, \mathbf{x}]$  (where  $\mathcal{U} = \mathcal{U}_1$ ) with a corresponding partition function

$$\mathcal{Z}_\theta[\mathbf{x}] = \int \mathcal{D}[\mathbf{s}] e^{-\mathcal{U}_\theta[\mathbf{s}, \mathbf{x}]}. \quad (40)$$

For instance, for  $0 \leq \theta \leq 1$ , we can define our potential to be

$$\mathcal{U}_\theta[\mathbf{s}, \mathbf{x}] = \mathcal{U}_0[\mathbf{s}, \mathbf{x}] + \theta \Delta\mathcal{U}[\mathbf{s}, \mathbf{x}], \quad (41)$$

such that  $e^{-\mathcal{U}_\theta[\mathbf{s}, \mathbf{x}]} = \mathcal{P}[\mathbf{s}]\mathcal{P}[\mathbf{x}|\mathbf{s}]^\theta$ . Note that this is the simplest choice for a continuous transformation between  $\mathcal{U}_0$  and  $\mathcal{U}_1$ , but by no means the only one. For reasons of computational efficiency it can be beneficial to choose a different path between  $\mathcal{U}_0$  and  $\mathcal{U}_1$ , depending on the specific system [46]. Here we will not consider other paths however, and derive the thermodynamic integration estimate for the potential given in Eq. (41).

To derive the thermodynamic integration estimate for the free-energy difference, we first compute the derivative of  $\ln \mathcal{Z}_\theta[\mathbf{x}]$  with respect to  $\theta$ :

$$\begin{aligned} \frac{\partial}{\partial \theta} \ln \mathcal{Z}_\theta[\mathbf{x}] &= \frac{1}{\mathcal{Z}_\theta[\mathbf{x}]} \frac{\partial}{\partial \theta} \int \mathcal{D}[\mathbf{s}] e^{-\mathcal{U}_\theta[\mathbf{s}, \mathbf{x}]} \\ &= - \left\langle \frac{\partial \mathcal{U}_\theta[\mathbf{s}, \mathbf{x}]}{\partial \theta} \right\rangle_\theta \\ &= - \langle \Delta\mathcal{U}[\mathbf{s}, \mathbf{x}] \rangle_\theta. \end{aligned} \quad (42)$$

Thus, the derivative of  $\ln \mathcal{Z}_\theta[\mathbf{x}]$  is an average of the Boltzmann weight with respect to  $\mathcal{P}_\theta[\mathbf{s}|\mathbf{x}]$  which is the ensemble distribution of  $\mathbf{s}$  given by

$$\mathcal{P}_\theta[\mathbf{s}|\mathbf{x}] = \frac{1}{\mathcal{Z}_\theta[\mathbf{x}]} e^{-\mathcal{U}_\theta[\mathbf{s},\mathbf{x}]} . \quad (43)$$

Integrating Eq. (42) with respect to  $\theta$  leads to the formula for the free-energy difference

$$\Delta\mathcal{F}[\mathbf{x}] = - \int_0^1 d\theta \langle \Delta\mathcal{U}[\mathbf{s},\mathbf{x}] \rangle_\theta \quad (44)$$

which is the fundamental identity underlying thermodynamic integration.

To compute the free-energy difference using Eq. (44), we evaluate the  $\theta$ -integral numerically using Gaussian quadrature, while the inner average is computed using a Monte Carlo simulation. The numerical integration requires the evaluation of the integrand for a sufficient number of different values of  $\theta$ . Therefore, we need to compute the average  $\langle \Delta\mathcal{U}[\mathbf{x}|\mathbf{s}] \rangle_{\mathcal{P}_\theta[\mathbf{s}|\mathbf{x}]}$  for any  $\theta \in [0, 1]$ .

These averages are evaluated using MCMC simulations in trajectory space using ideas from transition path sampling (TPS) [48]. However, as discussed in Appendix B, the efficiency of MCMC samplers strongly depends on the proposal moves that are employed. While better proposal moves could be conceived, we only use the *forward shooting* and *backward shooting* moves of TPS [48] to obtain the results in Section V. These moves regrow either the end, or the beginning of a trajectory, respectively. A proposal is accepted according to the Metropolis criterion [70].

#### IV. INTEGRATING OUT INTERNAL COMPONENTS

So far the output trajectory  $\mathbf{x}$  has been considered to correspond to the trajectory of the system in the *full* state space  $\Omega$ . Concomitantly, the method presented is a scheme for computing the mutual information between the input signal  $\mathbf{s}$  and the trajectory  $\mathbf{x}$ , comprising the time evolution of all the  $n$  components in the system,  $X^1, X^2, \dots, X^n$ . Each component  $X^i$  itself has a corresponding trajectory  $\mathbf{x}^i$ , such that the full trajectory can be represented as a vector  $\mathbf{x} = (\mathbf{x}^1, \dots, \mathbf{x}^n)$ . It is indeed also the conditional probability  $\mathcal{P}[\mathbf{x}|\mathbf{s}] = \mathcal{P}[\mathbf{x}^1, \dots, \mathbf{x}^n|\mathbf{s}]$  and the marginal probability  $\mathcal{P}[\mathbf{x}] = \mathcal{P}[\mathbf{x}^1, \dots, \mathbf{x}^n]$  of this vector in the full state space that can be directly computed from the master equation. In fact, it is this vector, which captures the states of all the components in the system, that carries the most information on the input signal  $\mathbf{s}$ , and thus has the largest mutual information. However, typically the downstream system cannot read out the states of all the components  $X^1, \dots, X^n$ . Often, the downstream system reads out only a few components or often even just one component, the “output component”  $X^r$ . The other components then mainly serve to

transmit the information from the input  $\mathbf{s}$  to this readout  $X^r$ . From the perspective of the downstream system, the other components are hidden. The natural quantity to measure the precision of information processing is then the mutual information  $I(\mathcal{S}; \mathcal{X}^r)$  between the input  $\mathbf{s}$  and the output component’s trajectory  $\mathbf{x}^r$ , not  $I(\mathcal{S}; \mathcal{X})$ . The question then becomes how to compute  $\mathcal{P}[\mathbf{x}^r]$  and  $\mathcal{P}[\mathbf{x}^r|\mathbf{s}]$ , from which  $I(\mathcal{S}; \mathcal{X}^r)$  can be obtained. Here, we present a scheme to achieve this.

As an example, consider a chemical reaction network with species  $X^1, \dots, X^n$ . Without loss of generality, we will assume that the  $n$ -th component is the output component,  $X^r = X^n$ . The other species  $X^1, \dots, X^{n-1}$  are thus not part of the output, but only relay information from the input signal  $\mathbf{s}$  to the output signal  $\mathbf{x}^n$ . Using our technique, to compute the mutual information  $I(\mathcal{A}, \mathcal{B})$  between two quantities  $\mathcal{A}, \mathcal{B}$  we need an expression for the corresponding conditional probability  $P(b|a)$ . Consequently, to compute the mutual information  $I(\mathcal{S}; \mathcal{X}^n)$  we need to compute  $\mathcal{P}[\mathbf{x}^n|\mathbf{s}]$  where  $\mathbf{x}^n$  is the trajectory of only the readout component  $X^n$ . Note that we cannot directly derive an expression for this conditional probability. Indeed, from the master equation of the whole jump process we merely get an expression for the full conditional probability  $\mathcal{P}[\mathbf{x}^1, \dots, \mathbf{x}^n|\mathbf{s}]$  of all components. Instead, we must compute the value of  $\mathcal{P}[\mathbf{x}^n|\mathbf{s}]$  by evaluating the marginalization integral

$$\mathcal{P}[\mathbf{x}^n|\mathbf{s}] = \int \mathcal{D}[\mathbf{x}^1] \cdots \int \mathcal{D}[\mathbf{x}^{n-1}] \mathcal{P}[\mathbf{x}^1, \dots, \mathbf{x}^n|\mathbf{s}] . \quad (45)$$

We can compute this integral using a Monte Carlo scheme as described below, and use the resulting estimate for  $\mathcal{P}[\mathbf{x}^n|\mathbf{s}]$  to compute the mutual information using our technique presented in Section II B.

To derive the Monte Carlo scheme for  $\mathcal{P}[\mathbf{x}^n|\mathbf{s}]$ , we observe that in Eq. (45) we use a marginalization to evaluate a marginal probability density by integrating out degrees of freedom from a known joint probability distribution. In Eq. (8) we solved the analogous problem of obtaining the marginal probability  $\mathcal{P}[\mathbf{x}]$  by integrating out the input trajectories through the integral  $\mathcal{P}[\mathbf{x}] = \int d\mathbf{s} \mathcal{P}[\mathbf{s}, \mathbf{x}] = \int d\mathbf{s} \mathcal{P}[\mathbf{s}] \mathcal{P}[\mathbf{x}|\mathbf{s}]$ . As we described in Section II B, the integral from Eq. (8) can be computed via a Monte Carlo estimate by sampling many input trajectories from  $\mathcal{P}[\mathbf{s}]$  and taking the average of the corresponding conditional probabilities  $\mathcal{P}[\mathbf{x}|\mathbf{s}_i]$ . We will show that in the case where there is no feedback from the readout component back to the other components, a completely analogous Monte Carlo estimate can be derived for Eq. (45). We describe this Monte Carlo estimate below. Additionally, in the absence of feedback, the techniques presented in Section III A above can be employed to develop a computationally more efficient scheme for the marginalization of the integral, Eq. (45).

More specifically, we can evaluate Eq. (45) via a direct Monte Carlo estimate under the condition that the stochastic dynamics of the other components  $X^1, \dots, X^{n-1}$  are not influenced by  $X^n$  (i.e. no feedback

from the readout). Using the identity

$$\mathcal{P}[\mathbf{x}^1, \dots, \mathbf{x}^n | \mathbf{s}] = \mathcal{P}[\mathbf{x}^1, \dots, \mathbf{x}^{n-1} | \mathbf{s}] \mathcal{P}[\mathbf{x}^n | \mathbf{x}_i^1, \dots, \mathbf{x}_i^{n-1}, \mathbf{s}] \quad (46)$$

to rewrite the integrand in Eq. (45), we are able to represent the conditional probability  $\mathcal{P}[\mathbf{x}^n | \mathbf{s}]$  as an average over the readout component's trajectory probability

$$\mathcal{P}[\mathbf{x}^n | \mathbf{s}] = \langle \mathcal{P}[\mathbf{x}^n | \mathbf{x}_i^1, \dots, \mathbf{x}_i^{n-1}, \mathbf{s}] \rangle_{\mathcal{P}[\mathbf{x}^1, \dots, \mathbf{x}^{n-1} | \mathbf{s}]} \cdot \quad (47)$$

Thus, assuming that we can evaluate the conditional probability of the readout given all the other components,  $\mathcal{P}[\mathbf{x}^n | \mathbf{x}_i^1, \dots, \mathbf{x}_i^{n-1}, \mathbf{s}]$ , we arrive at the Monte Carlo estimate

$$\mathcal{P}[\mathbf{x}^n | \mathbf{s}] \approx \frac{1}{M} \sum_{i=1}^M \mathcal{P}[\mathbf{x}^n | \mathbf{x}_i^1, \dots, \mathbf{x}_i^{n-1}, \mathbf{s}] \quad (48)$$

where the samples  $\mathbf{x}_i^1, \dots, \mathbf{x}_i^{n-1}$  for  $i = 1, \dots, M$  are drawn from  $\mathcal{P}[\mathbf{x}^1, \dots, \mathbf{x}^{n-1} | \mathbf{s}]$ . Notice that the derivation of the Monte Carlo estimate is fully analogous to the estimate in Eq. (8), but instead of integrating out the input trajectory  $\mathbf{s}$  we marginalize out the component trajectories  $\mathbf{x}^1, \dots, \mathbf{x}^{n-1}$ .

To obtain  $\mathcal{P}[\mathbf{x}^n | \mathbf{x}_i^1, \dots, \mathbf{x}_i^{n-1}, \mathbf{s}]$  in Eqs. (47) and (48), we note that, in absence of feedback, we can describe the stochastic dynamics of the readout component  $X^n$  as a jump process with time-dependent transition rates whose time-dependence arises from the trajectories of the other components  $\mathbf{x}^1, \dots, \mathbf{x}^{n-1}$  and the input trajectory  $\mathbf{s}$ . In effect, this is a driven jump process for  $X^n$ , driven by all upstream components  $X^1, \dots, X^{n-1}$  and also by the input signal. Specifically, denoting  $\mathbf{u} = (\mathbf{x}^1, \dots, \mathbf{x}^{n-1}, \mathbf{s})$  as the joint trajectory representing the history of all upstream components as well as the input signal, we can, as explained in Section II C, write the time dependent transition rate matrix  $Q_i(\cdot | \mathbf{u})$  for the stochastic dynamics of  $X^n$  and use Eq. (15) to compute  $\mathcal{P}[\mathbf{x}^n | \mathbf{u}] = \mathcal{P}[\mathbf{x}^n | \mathbf{x}_i^1, \dots, \mathbf{x}_i^{n-1}, \mathbf{s}]$ . Using Eq. (48), this then allows us to compute  $\mathcal{P}[\mathbf{x}^n | \mathbf{s}]$ .

Finally, to compute the mutual information  $I(\mathcal{S}; \mathcal{X}^n)$  e.g. using the estimate in Eq. (10) we additionally need to evaluate the marginal output probability  $\mathcal{P}[\mathbf{x}^n]$ . This requires us to perform one additional integration over the space of input trajectories  $\mathbf{s}$ :

$$\begin{aligned} \mathcal{P}[\mathbf{x}^n] &= \int \mathcal{D}[\mathbf{s}] \mathcal{P}[\mathbf{s}] \mathcal{P}[\mathbf{x}^n | \mathbf{s}] \\ &= \langle \mathcal{P}[\mathbf{x}^n | \mathbf{s}] \rangle_{\mathcal{P}[\mathbf{s}]} \cdot \end{aligned} \quad (49)$$

The corresponding Monte Carlo estimate is

$$\begin{aligned} \mathcal{P}[\mathbf{x}^n] &\approx \frac{1}{N} \sum_{i=1}^N \mathcal{P}[\mathbf{x}^n | \mathbf{s}_i] \\ &\approx \frac{1}{N} \sum_{i=1}^N \frac{1}{M} \sum_{j=1}^M \mathcal{P}[\mathbf{x}^n | \mathbf{x}_{ij}^1, \dots, \mathbf{x}_{ij}^{n-1}, \mathbf{s}_i] \end{aligned} \quad (50)$$

with input trajectories  $\mathbf{s}_i \sim \mathcal{P}[\mathbf{s}]$  and  $(\mathbf{x}_{ij}^1, \dots, \mathbf{x}_{ij}^{n-1}) \sim \mathcal{P}[\mathbf{x}^1, \dots, \mathbf{x}^{n-1} | \mathbf{s}_i]$  for  $i = 1, \dots, N$  and  $j = 1, \dots, M$ .

In summary, the scheme to obtain  $\mathcal{P}[\mathbf{x}^n | \mathbf{u}]$  in the presence of hidden intermediate components is analogous to that used for computing  $\mathcal{P}[\mathbf{x}]$  from  $\mathcal{P}[\mathbf{x} | \mathbf{s}]$ . In both cases, one needs to marginalize a distribution function by integrating out a component, either the input  $\mathbf{s}$  and/or the intermediate components  $X^1, \dots, X^n$ . Indeed, the scheme presented in Section II B and the scheme presented here are bona fide schemes to compute the mutual information between the input  $\mathbf{s}$  and either the full output  $\mathbf{x}$  or the trajectory of the output component  $\mathbf{x}^n$ . However, when the trajectories are sufficiently long or the stochastic dynamics are sufficiently complex, then in both cases the efficiency of computing the marginalized distribution,  $\mathcal{P}[\mathbf{x}]$  or  $\mathcal{P}[\mathbf{x}^n | \mathbf{s}]$ , is a concern. In this case, the schemes to compute free-energy differences discussed in Section III can be used.

## V. RESULTS

To demonstrate the power of our framework and to illustrate how the techniques of the previous sections can be applied, we apply PWS to two instructive chemical reaction networks. We first consider a linearly coupled birth-death process. This system has already been studied previously using a Gaussian model [6], and by Duso and Zechner [30] using an approximative technique, and we compare our results to those of these studies. This simple birth-death system serves to illustrate the main ideas of our approach and also highlights, as we will see, that linear systems can be distinctly non-Gaussian. The second example has been chosen to demonstrate the practical applicability of our technique. We use RR-PWS to compute the mutual information rate in the bacterial chemotaxis system, which is not only one of the best characterized signaling systems in biology, but is also a prime example of a complex information processing system consisting of many reactions.

The code used to produce the PWS estimates was written in the Julia programming language [71] and has been made freely available online [72]. For performing stochastic simulations we use the DifferentialEquations.jl package [73] and biochemical reaction models are set up with help from the ModelingToolkit.jl package [74].

### A. Coupled Birth-Death Processes

As a first example system we consider a very simple birth-death process  $\emptyset \rightleftharpoons X$  which describes a member of species  $X$  being created at rate  $\rho(t)$  and its decay with constant rate  $\mu$ . This system receives information from an input signal which modulates the rate  $\rho(t)$ . For simplicity we assume that the dependence of the birth rate

of  $X$  on the input level is given by the linear relation

$$\rho(t) = \rho_0 s(t) \quad (51)$$

where  $\rho_0$  is a constant and  $s(t)$  is the input copy number at time  $t$ . This is a simple model for gene expression, where the rate of production of a protein  $X$  is controlled by a transcription factor  $S$ , and  $X$  itself has a characteristic decay rate. The input trajectories  $s(t)$  themselves are generated from a separate birth-death process  $\emptyset \rightleftharpoons S$ . We assume that the creation and decay rates for  $S$  are constants  $\kappa$  and  $\lambda$ , respectively.

We compute the trajectory mutual information for this system as a function of the trajectory duration  $T$  of input and output trajectories. Naturally, the mutual information increases with the trajectory duration. For  $T \rightarrow \infty$ , the trajectory mutual information is expected to increase linearly with  $T$ , since, on average, every additional output segment contains the same additional amount of information on the input trajectory.

Specifically, we studied the mutual information of this system in steady state. Therefore, we set the initial condition  $P(s_0, x_0)$  as the stationary distribution of the combined two-component jump system with species  $(S, X)$  which was obtained using a Gaussian approximation. Note that the choice of initial condition does not influence the asymptotic rate of increase of the mutual information, but leads to a nonzero mutual information already for  $T = 0$ .

Figure 4 shows the results of our scheme for computing the trajectory mutual information when applied to the simple birth-death process described above. We compare the results obtained using our techniques with each other, and with the trajectory mutual information obtained by the approximative scheme from Duso and Zechner [30]. To perform the latter computation, we used the code publicly provided by the authors [75], and to avoid making modifications to this code, we chose a slightly different, fixed initial condition ( $s_0 = x_0 = 50$ ) which leads to the mutual information being zero for  $T = 0$ . Finally, for comparison, we also show the analytical result of a Gaussian model, obtained using the linear noise approximation, see Appendix D.

Our results show that for short trajectories, all marginal probability estimation schemes lead to a convergent estimate of the mutual information between input and output trajectories. However, for longer trajectories, the brute force sampler and—to a smaller extent—the thermodynamic integration estimate suffer from systematic bias due to undersampling. Indeed, in both cases, we over-estimate the mutual information when compared to the results from RR-PWS. For the brute force algorithm DPWS, as we increase the number  $M$  of input trajectories used for the marginalization integral, this systematic error decreases. Similarly, for TI-PWS the systematic error decreases as we use more MCMC samples for the marginalization scheme. For the RR-PWS however, already for  $M = 128$  the estimate arises without systematic error and we checked that a further increase of  $M$  does

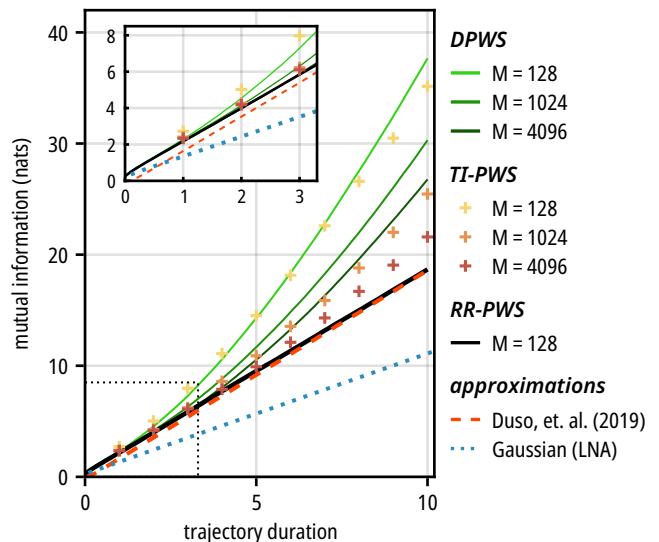


FIG. 4. Comparing different schemes to compute the mutual information as a function of trajectory duration for a simple coupled birth-death process with rates  $\kappa = 50, \lambda = 1, \rho_0 = 10, \mu = 10$  and steady-state initial condition. The inset shows an enlarged version of the dotted rectangle near the origin. For short trajectories all PWS estimates agree. Yet, for longer trajectories, DPWS and TI-PWS require a much larger number of input trajectories  $M$  for computing  $\mathcal{P}[\mathbf{x}]$  than RR-PWS, in order to converge. Results for the three PWS variants are compared with the Duso and Zechner [30] estimate, and with the linear noise approximation from Ref. [6]. Due to a different choice of initial condition, the Duso scheme initially underestimates the mutual information, but otherwise we find excellent agreement between it and RR-PWS. The linear noise approximation systematically underestimates the mutual information. All PWS estimates, as well as the Duso approximation were computed using  $N = 10^4$  samples from  $\mathcal{P}[\mathbf{s}, \mathbf{x}]$ .

not change the results.

We also find excellent agreement between the results of the approximative scheme by Duso and Zechner [30] and the RR-PWS estimate. Only very small deviations are visible in Fig. 4. These deviations are mostly caused by the different choice of initial conditions. Since, in contrast to the PWS estimates, the computation via the Duso scheme is performed with a fixed initial condition the trajectory mutual information is zero for  $T = 0$ , i.e. slightly lower than that obtained by RR-PWS, where the mutual information at  $T = 0$  is determined by the steady state distribution  $P(s_0, x_0)$ . Yet, as  $T$  increases the Duso estimate slowly “catches up” to the RR-PWS result.

For comparison, we have also shown the prediction of the Gaussian (linear noise) model of the same reaction network, as described in Ref. [6]. Interestingly, while this birth-death process is a linear system, the Gaussian model underestimates the mutual information for  $T > 0$  (for the initial condition at  $T = 0$  the Gaussian model matches the PWS results). Although a full analysis of this result is beyond the scope of this manuscript, we do

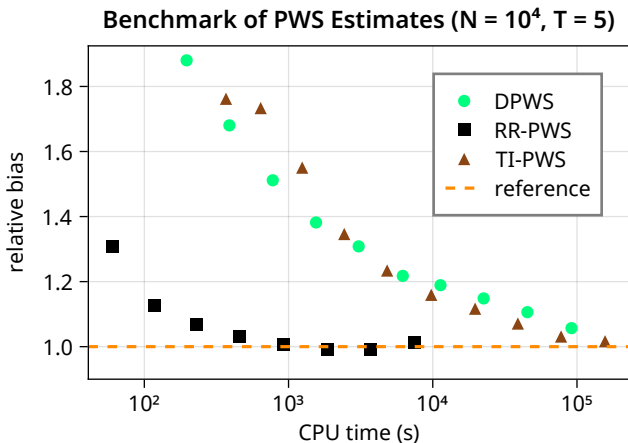


FIG. 5. Comparing estimation bias for the different PWS variants in relation to their CPU time requirements. Each dot represents a single mutual information estimate with  $N = 10^4$  samples for trajectories of duration  $T = 5$ . Almost all the CPU time of a PWS estimate is spent on the computation of the marginal probability  $\mathcal{P}[\mathbf{x}]$ . The bias of the marginal probability estimate can be reduced by using a larger number  $M$  of sampled input trajectories to compute the marginalization integral, which also increases the required CPU time. The RR-PWS estimate converges much faster than the estimate of DPWS and TI-PWS. For DPWS and TI-PWS, the dots represents estimates ranging from  $M = 2^5$  to  $M = 2^{14}$ , for RR-PWS ranging from  $M = 2^3$  to  $M = 2^{10}$ . As the baseline of zero bias we use the converged result from the RR-PWS estimates.

note here that this is not a consequence of small copy number fluctuations: increasing the average copy number does not significantly improve the Gaussian estimate. This simple example thus shows that the Gaussian approximation should be used with care in computing the mutual information between trajectories, even when the reaction network is linear. A similar observation was made in Ref. [25].

The three different PWS methods differ in their approach to compute the marginal probability  $\mathcal{P}[\mathbf{x}]$  and thus differ in computational efficiency. In Fig. 5, as a benchmark, we show the magnitude of the systematic error of the different PWS estimates in relation to the required CPU time. Indeed, as expected, the computation of the marginal probability poses problems for long trajectories when using the brute force Direct PWS scheme. More interestingly, while TI-PWS improves the estimate of the mutual information, the improvement is not dramatic. Unlike the brute-force scheme, thermodynamic integration does make it possible to generate input trajectories  $\mathbf{s}$  that are correlated with the output trajectories  $\mathbf{x}$ , namely according to  $\mathcal{P}_\theta[\mathbf{s}|\mathbf{x}]$ , but it still overestimates the mutual information for long trajectories unless a very large number of MCMC samples is used.

The RR-PWS implementation evidently outperforms the other estimates for this system. Clearly, the regular

resampling steps in the particle filter algorithm ensure that we mostly sample input trajectories  $\mathbf{s}$  with non-vanishing likelihood  $\mathcal{P}[\mathbf{x}|\mathbf{s}]$ , thereby avoiding the under-sampling problem from the brute force scheme. Moreover, sequential Monte Carlo techniques like RR-PWS and FFS [66] have a considerable advantage over MCMC techniques for sampling trajectories from the  $\mathcal{P}[\mathbf{s}|\mathbf{x}]$  ensemble. With MCMC path sampling, we frequently make small changes to an existing trajectory such that the system moves slowly in path space, leading to poor statistics. In contrast, in RR-PWS we generate new trajectories from scratch, segment by segment, and these explore the trajectory space much faster.

While a coupled birth-death process represents a simple yet non-trivial system capable of information transmission, we show in the next section that the PWS approach can be applied to complex and more realistic information transmitting systems, such as cellular signaling networks with many components and chemical reactions.

## B. Bacterial Chemotaxis

The chemotaxis system of the bacterium *Escherichia coli* is a complex information processing system that is responsible for detecting nutrient gradients in the cell's environment and using that information to guide the bacterium's movement. Briefly, *E. coli* navigates through its environment by performing a biased random walk, successively alternating between so-called *runs*, during which it swims with a nearly constant speed, and *tumbles*, during which it chooses a new direction [76]. The rates of switching between these two states are controlled by the chemotaxis sensing system, see Fig. 6a. This system consists of receptors on the cell surface that detect the ligand, and a downstream signaling network that processes this information by taking the time-derivative of the signal, the ligand concentration. This derivative is taken via two antagonistic reactions, which occur on two distinct timescales. Attractant binding rapidly deactivates the receptor, while slow methylation counteracts this reaction by reactivating the receptor, leading to near perfect adaptation [77–80]. Lastly, active receptors phosphorylate the downstream messenger protein CheY, which controls the tumbling propensity by binding the flagellar motors that propel the bacterium.

In our model, the receptors are grouped in clusters (Appendix E). Each receptor can switch between an active and an inactive conformational state, but, in the spirit of the Monod-Wyman-Changeux model [81], the energetic cost of having two different conformations in the same cluster is prohibitively large. We can then speak of each cluster as either being active or inactive. Each receptor in a cluster can bind ligand and be (de)methylated, which, together, control the probability that the cluster is active. In addition, the receptor clusters can phosphorylate CheY, while phosphorylated CheY is dephosphorylated at a constant rate. The kinase

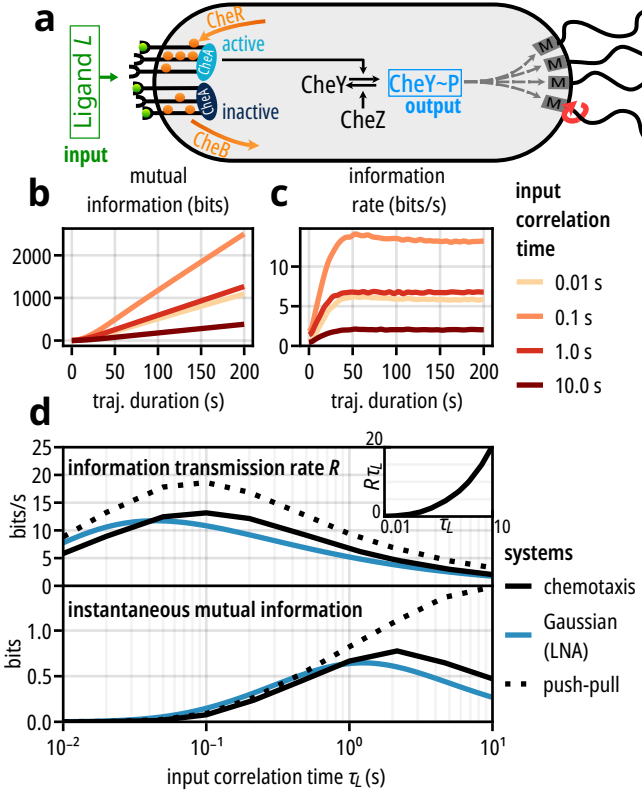


FIG. 6. The information transmission rate in the chemotaxis system. **a** Cartoon of the chemotaxis network of *E. coli*. Receptors form clusters with an associated CheA kinase. A cluster can either be active or inactive, depending on the number of bound ligands (green dots) and methylated sites (orange dots). Active CheA can phosphorylate CheY; phosphorylated CheY controls the rotation direction of the flagellar motors and thereby the movement of the bacterium. **b** Trajectory mutual information as a function of trajectory length for inputs with different correlation times  $\tau_L$ . For each RR-PWS simulation,  $N = 3600$  input-output pairs  $(s, \mathbf{x})$  were sampled ( $M = 128$  for the particle filter). **c** Information transmission rate  $\partial_T I(\mathcal{L}_T, \mathcal{X}_T)$ , i.e. the increase of mutual information per unit increment of trajectory duration. **d** The information transmission rate  $R \equiv \lim_{T \rightarrow \infty} \partial_T I(\mathcal{L}_T, \mathcal{X}_T)$  and the instantaneous mutual information  $I_{\text{inst}}(L; X)$  for the full chemotaxis system and that without the adaption system, i.e. the push-pull network. While  $R$  correctly predicts the optimal input correlation time  $\tau_L$ ,  $I_{\text{inst}}(L; X)$  does not. The Gaussian (LNA) approximation suffers from uncontrolled biases, by over- or under-estimating the true rate depending on  $\tau_L$ . The inset shows that while  $R$  varies non-monotonically with the input correlation time  $\tau_L$ , the information harvested during  $\tau_L$ ,  $R\tau_L$ , rises monotonically.

CheA and the phosphatase CheZ are thus not modeled explicitly. Due to the combinatorial explosion of receptor states within each cluster, the system has 173 elementary reactions.

The input signal represents the ligand concentration, which is modeled as a simple birth-death process  $\emptyset \rightleftharpoons L$ . The dynamics of this process are fully described by

two parameters, the steady-state mean copy number of ligands  $\bar{L}$ , and the correlation time  $\tau_L$ ; the variance  $\sigma_L^2$  of this signal equals the mean  $\bar{L}$ . The output signal is the concentration of phosphorylated CheY. The receptor states are thus the hidden internal states, and we use the technique of Section IV to integrate out these hidden states. For a more detailed description of the system and the model parameters see Appendix E.

Figure 6b shows how the mutual information increases with trajectory duration for our chemotaxis system for input signals with different correlation times  $\tau_L$ . In all cases, it is seen that after a transient, the mutual information  $I(\mathcal{L}_T, \mathcal{X}_T)$  between the ligand trajectories  $\mathcal{L}_T$  and the CheY-P trajectories  $\mathcal{X}_T$  rises linearly with trajectory duration  $T$ , as expected. The information rate  $\partial_T I(\mathcal{L}_T, \mathcal{X}_T)$  in Fig. 6c first increases quickly and subsequently decreases towards a plateau. This behavior is determined by the relationship between input entropy rate  $\partial_T H(\mathcal{L}_T)$  and the *conditional* input entropy rate  $\partial_T H(\mathcal{L}_T | \mathcal{X}_T)$ . The former initially increases relatively fast before reaching a plateau, because the input reaches its steady state quickly, on the timescale of  $\tau_L$ . The latter only reaches its plateau once the system has fully relaxed to its steady state, i.e. at the methylation timescale  $\tau_m \approx 10$  s. Thus, for  $\tau_L \ll \tau_m$  the input entropy rate initially rises faster than the conditional input entropy rate, leading to a transient peak in the information rate (hence, for  $\tau_L = 10$  s there is no peak since input and output relax at approximately the same speed).

Mattingly *et al.* [52] recently showed that *E. coli* chemotaxis is limited by information transmission. Yet, the authors used a Gaussian model to measure the information transmission rate. The question therefore remains how accurate this model is for the chemotaxis system, especially given the fact that for the birth-death system analyzed above the Gaussian model underestimates the rate by a factor of 2. Fig. 6d shows that for the chemotaxis system the Gaussian model is, in fact, surprisingly accurate: the rate predicted by the Gaussian model deviates by no more than 50% from the exact result computed by PWS. However, the deviation is not consistent—the Gaussian model overestimates the rate for some input frequencies while it underestimates it for others—and the predicted optimal input correlation time is markedly off, by a factor of 2. The approximations of the Gaussian model are not controlled, and care should thus be taken in employing this model for computing the information transmission rate.

Our results demonstrate an important principle for fast information transmission: the dynamics of the processing system and its input signal must be matched. In particular, Fig. 6d shows that there exists an optimal correlation time of the input signal of  $\tau_L \approx 0.1$  s that maximizes the information transmission rate. A shorter input correlation time increases the number of independent messages that are transmitted per unit amount of time, which tends to raise the information transmission rate by increasing the input signal's entropy  $H(\mathcal{L})$  (cf. Eq. (2)).



On the other hand, a shorter input correlation time also means that the input signal varies more rapidly in time, which makes it harder to track by the processing system; this tends to reduce the information transmission rate by increasing the conditional entropy of the input  $H(\mathcal{L}|\mathcal{X})$ . The interplay between these two opposing effects gives rise to an optimal input correlation time that maximizes the information rate. These arguments are generic and apply to any information-processing system [21].

Importantly, the information transmission rate is the appropriate information measure to address the question whether a system is matched to its input dynamics. Other measures neither make it possible to address that question quantitatively nor qualitatively. For instance, the widely used Instantaneous Mutual Information (IMI) between the steady state input and output at a given time point [6, 14, 82–85] predicts an optimal input correlation time of  $\tau_L \approx 2$  s, about an order of magnitude larger than that which maximizes the information transmission rate (Fig. 6d). Moreover, this optimum does not imply optimal information transmission, because it has a completely different origin. The IMI decreases for more slowly varying input signals, not because this lowers the rate of independent input messages—this effect is not captured by the IMI—but because of the adaptation system of receptor methylation, which acts as a high-pass filter at the methylation time scale  $\tau_m \approx 10$  s.

To demonstrate this, we consider the chemotaxis system without the adaptation system, reducing it to a canonical push-pull network, a common motif in cell signaling. Indeed, without the adaptation system the IMI rises monotonically with  $\tau_L$ . In contrast, the information transmission rate still exhibits an optimal input correlation time, because, unlike the IMI, it captures the generic trade-off between maximizing the frequency of input messages and transmitting these messages reliably. To properly take into account the effect of correlations in the input signal on information transmission, it is paramount to consider the mutual information between input and output trajectories, like the information transmission rate does.

Comparing the information transmission rate between the chemotaxis system and the push-pull network reveals two other points worthy of note. The first is that the optimal input correlation time is nearly identical in these two systems, showing that the information on the time-varying input signal is predominantly relayed via the phosphorylation dynamics of CheY. Interestingly, while this optimal input timescale of  $\approx 100$  ms is smaller than the typical run duration of *E. coli* in the absence of any concentration gradient, which is about a second [86, 87], it is comparable to the timescale of CheYp-motor binding [88] and that of fast motor switching [89]. This indicates that the optimal input correlation time is physiologically relevant, e.g. for inducing a rapid repellent response, which indeed happens on a timescale of 100 ms [90]. Yet, the question remains what the relevant information is for chemotactic performance, as measured for example

by the drift velocity in an exponential gradient. It has been argued that this is the information collected during the signal correlation time  $\tau_L$ , which is the information transmission rate  $R$  times  $\tau_L$  [6, 52]. Interestingly, while  $R$  varies non-monotonically with  $\tau_L$ , the product  $R\tau_L$  increases with  $\tau_L$  (inset Fig. 6d). This result suggests it is beneficial to increase the run duration  $\tau_R$ , because this increases  $\tau_L$  in the physiologically relevant regime where  $\tau_R$  is shorter than the orientational diffusion time [52]. Clearly, how chemotactic performance depends on the information transmission rate, and in particular whether there is a trade-off between responding fast and responding reliably, is an important topic for further study.

The second point is that the chemotaxis system has a lower information transmission rate than the push-pull network, for all input timescales. The combination of fast signaling and slow adaptation allows the chemotaxis system to take a temporal derivative of the input signal [11], which is optimal for predicting non-Markovian signals [82]. The experiments of Mattingly *et al.* [52] indicate however that the input signal for a bacterium swimming in an exponential gradient is to a good approximation Markovian, as we have assumed here. Our results show that while the adaptation system enables the bacterium to sense over a wide range of background concentrations, it comes at the cost of reducing the information transmission rate. An intriguing question for future research is whether this observation reflects a generic trade-off between these requirements.

## VI. DISCUSSION

Our analysis of the bacterial chemotaxis system shows the importance of employing the appropriate information measure to quantify and characterize the flow of information. This measure is the mutual information between trajectories, or its temporal derivative, the information transmission rate. Computing it exactly has, however, so far remained elusive. In this manuscript, we have developed a general, practical and flexible method that makes it possible to compute the mutual information between trajectories exactly for any system described by a master equation. PWS is a Monte Carlo scheme that is based on the exact computation of trajectory probabilities from the master equation. Since the master equation is employed in many fields and in particular provides an exact stochastic model for well-mixed chemical reaction dynamics, PWS is very broadly applicable.

While we have applied PWS to compute the mutual information (rate) in steady state, PWS can be used equally well to study systems out of steady state. For such systems a (non-)equilibrium initial condition  $P(s_0, x_0)$  must be specified in addition to a well-defined non-stationary probability distribution of input trajectories  $\mathcal{P}[\mathbf{s}]$ . These distributions are defined by the (experimental) setup, and lead to a well-defined output distribution  $\mathcal{P}[\mathbf{x}]$  when the system is coupled to the input.

Thus, a steady state is no prerequisite for the application of PWS to study the trajectory mutual information.

Throughout the manuscript we have considered systems in which the output does not feed back onto the input. In systems with feedback, the current output influences future input, which means that we cannot straightforwardly generate input trajectories according to  $\mathcal{P}[\mathbf{s}]$ . Moreover,  $\mathcal{P}[\mathbf{x}|\mathbf{s}]$ , the central quantity of all three PWS methods, cannot be obtained straightforwardly. Nonetheless, PWS can be extended to systems with feedback as shown in Appendix C. As in free-energy calculations, the trick is to define a reference system for which the marginal probability distribution—and thus the “free energy”—is known and then compute the “free-energy difference” between that reference system and the system of interest.

Given that PWS makes it possible to compute the mutual information between trajectories of pure jump processes described by a master equation, it is natural to wonder if this concept can be extended to other types of stochastic processes. At the core of the PWS method is the exact evaluation of the path likelihood  $\mathcal{P}[\mathbf{x}|\mathbf{s}]$  from the master equation. Therefore, in order to use PWS with a different stochastic process, we require the ability to compute the path likelihood  $\mathcal{P}[\mathbf{x}|\mathbf{s}]$  for its sample paths. Remarkably, for *stochastic diffusion processes*, which are described by a Langevin equation in a continuous state space, the trajectory probability can be computed by replacing the kernel  $\mathcal{L}_t(\mathbf{s}, \mathbf{x})$  in Eq. (16) with the Onsager-Machlup function [91]. In particular, while the path probability is not well-defined for continuous sample paths, Adib [92] shows that the Onsager-Machlup function yields a correct expression for the path probability of time-discretized diffusion trajectories. Therefore, we expect that PWS can be straightforwardly extended to handle systems described by a Langevin equation. In such a PWS scheme, the Gillespie simulations are replaced by standard numerical integration techniques for Langevin equations (see e.g. Ref. [60]), and the trajectory likelihood is evaluated using the Onsager-Machlup function.

Aside from the DPWS scheme, we developed two additional variants of PWS, capitalizing on the connection between information theory and statistical physics. Specifically, the computation of the mutual information requires the evaluation of the marginal probability of individual output trajectories  $\mathcal{P}[\mathbf{x}]$ . This corresponds to the computation of a partition function in statistical physics. RR-PWS and TI-PWS are based on techniques from polymer and rare-event sampling to make the computation of the marginal trajectory probability more efficient.

The different PWS variants share some characteristics yet also differ in others. DPWS and arguably also RR-PWS are static Monte Carlo schemes, in which the trajectories are generated independently from the previous ones. These methods are similar to static polymer sampling schemes like PERM [43] and rare-event methods like DFFS or BG-FFS [66]. In contrast, TI-PWS is a

dynamic Monte Carlo scheme, where a new trajectory is generated from the previous trajectory. In this regard, this method is similar to the CBMC scheme for polymer simulations [93], and the TPS [48], TIS [94], and RB-FFS [66] schemes to harvest transition paths. The benefit of static schemes is that the newly generated trajectories are uncorrelated from the previous ones, which means that they are less likely to get stuck in certain regions of path space. Concomitantly, they tend to diffuse faster through the configuration space. Indeed, TI-PWS suffers from a problem that is also often encountered in TPS or TIS, which is that the middle sections of the trajectories move only very slowly in their perpendicular direction. The tricks that have been applied to TPS and TIS to solve this problem, like parallel tempering, could also be of use here [95].

Another distinction is that RR-PWS generates all the trajectories in the ensemble simultaneously yet segment by segment, like D-FFS, while DPWS and TI-PWS generate only one full trajectory at the time, similar to RB-FFS, BG-FFS, and also TPS and TIS. Consequently, RR-PWS, like D-FFS, faces the risk of *genetic drift*, which means that, after sufficiently many resampling steps most paths of the ensemble will originate from the same initial seed. Thus, when continuing to sample new segments, the old segments that are far in the past become essentially fixed, which makes it possible to miss important paths in the RR-PWS sampling procedure. This risk is likely to be more severe for systems that respond to the input signal with a significant delay. As in D-FFS, the risk of genetic drift can be mitigated by increasing the initial number of path segments. While we did not employ this trick here, we found that RR-PWS was by far the most powerful scheme of the three variants studied.

Overall, PWS is a general framework for computing the mutual information between trajectories. We presented three variants of PWS for systems described by a master equation. Apart from these we expect that other variants could be developed to improve efficiency for particular applications. Because of its flexibility and simplicity, we envision that the PWS will become an important and reliable tool to study information transmission in dynamic stochastic systems.

## ACKNOWLEDGMENTS

We thank Bela Mulder, Tom Shimizu, Peter Bolhuis, and Daan Frenkel for useful discussions and a careful reading of the manuscript and we thank Age Tjalma for support with obtaining the linear noise approximation of the chemotaxis system. This work is part of the Dutch Research Council (NWO) and was performed at the research institute AMOLF. This project has received funding from the European Research Council (ERC) under the European Union’s Horizon 2020 research and innovation program (grant agreement No. 885065), and was financially supported by NWO through the

“Building a Synthetic Cell (BaSyC)” Gravitation grant (024.003.019).

### Appendix A: Justification for the Particle Filter from Section IIIB

Here we justify the marginal probability estimate shown in Eq. (38), i.e. we show that the bootstrap particle filter used in Section IIIB provides a consistent estimate for the ratio of partition functions  $\mathcal{P}[\mathbf{x}] = \mathcal{Z}[\mathbf{x}]/\mathcal{Z}_0[\mathbf{x}]$ . The result that this estimate is also *unbiased* is more difficult to establish, a proof is given by Del Moral [96].

To make the derivations below easy to follow, we structure our justification of the particle filter into three steps. We first give a brief description of how a resampling procedure can generally be used to generate samples according to a target distribution when only samples from a different distribution are available. Secondly, we use these insights to explain how the resampling procedure used in the particle filter generates trajectories that are distributed approximately according to  $\mathcal{P}[\mathbf{s}|\mathbf{x}]$ , even though we only generate trajectories according to  $\mathcal{P}[\mathbf{s}]$ . Finally, we use this result to show that the particle filter provides a consistent estimate for  $\mathcal{P}[\mathbf{x}]$ .

#### 1. Sampling and Resampling

Sampling and then resampling is a strategy to use samples  $\mathbf{s}^1, \dots, \mathbf{s}^M$  from a given prior distribution  $f[\mathbf{s}]$  to generate *approximate* samples from a different distribution of interest, with density proportional to the product  $h[\mathbf{s}] = f[\mathbf{s}]g[\mathbf{s}]$ . In general,  $h[\mathbf{s}]$  is not normalized and we denote the corresponding normalized probability density by  $\hat{h}[\mathbf{s}] = h[\mathbf{s}]/\int \mathcal{D}[\mathbf{s}]h[\mathbf{s}]$ . To generate samples from  $\hat{h}[\mathbf{s}]$ , we assign each of the existing samples from  $f[\mathbf{s}]$  a normalized weight

$$W^k = \frac{g[\mathbf{s}^k]}{\sum_{j=1}^M g[\mathbf{s}^j]}. \quad (\text{A1})$$

Then, by sampling from the discrete set  $\{\mathbf{s}^1, \dots, \mathbf{s}^M\}$  according to the weights  $W^1, \dots, W^M$ , we pick samples that are approximately distributed according to  $\hat{h}[\mathbf{s}]$ . Indeed, for  $M \rightarrow \infty$  the distribution of the resulting samples approaches the density  $\hat{h}[\mathbf{s}]$  [97]. We use resampling at each iteration of the algorithm of Section IIIB to regularly prune those trajectories with low overall contribution to the marginalization integral.

#### 2. Distribution of Trajectories in the Particle Filter

In the bootstrap particle filter, at each iteration we start out with a set of trajectories  $\mathbf{s}_{[0,i-1]}^1, \dots, \mathbf{s}_{[0,i-1]}^M$

which we assume are approximately distributed according to  $\mathcal{P}[\mathbf{s}_{[0,i-1]}|\mathbf{x}_{[0,i-1]}]$ . In each iteration of the particle filter, the goal is to produce a set of trajectories approximately distributed according to  $\mathcal{P}[\mathbf{s}_{[0,i]}|\mathbf{x}_{[0,i]}]$ . Clearly, by iterating such a procedure we can generate a set of trajectories distributed approximately according to  $\mathcal{P}[\mathbf{s}_{[0,n]}|\mathbf{x}_{[0,n]}]$  for any  $n > 1$ . Note that we always carefully use the phrase *approximately distributed* because as explained above, for finite  $M$  a resampling procedure cannot generate *exact* samples from a probability distribution (yet the estimate for  $\mathcal{P}[\mathbf{x}]$  remains unbiased regardless of how good these approximations are). We now take a closer look at one iteration of the particle filter.

We start with the set of trajectories with time span  $[\tau_0, \tau_{i-1}]$ , denoted by  $\{\mathbf{s}_{[0,i-1]}^1, \dots, \mathbf{s}_{[0,i-1]}^M\}$ . These trajectories are then propagated forward to time  $\tau_i$ , by adding a new segment  $\mathbf{s}_{[i-1,i]}^k$  to trajectory  $\mathbf{s}_{[0,i-1]}^k$  for  $k = 1, \dots, M$ . Each new segment is generated from the distribution  $\mathcal{P}[\mathbf{s}_{[i-1,i]}^k|\mathbf{s}_{[0,i-1]}^k]$  such that the propagation step results in a set of trajectories  $\{\mathbf{s}_{[0,i]}^1, \dots, \mathbf{s}_{[0,i]}^M\}$ , distributed according to  $f[\mathbf{s}_{[0,i]}] = \mathcal{P}[\mathbf{s}_{[0,i]}|\mathbf{x}_{[0,i-1]}]$ .

Next, we resample from the set of trajectories, with the goal of producing a set of trajectories by distributed according to the target density  $\hat{h}[\mathbf{s}] = \mathcal{P}[\mathbf{s}_{[0,i]}|\mathbf{x}_{[0,i]}]$ . Thus, we have to find the appropriate weighting function  $g[\mathbf{s}_{[0,i]}]$  in order to approximately produce samples according to the target distribution. By choosing  $g[\mathbf{s}_{[0,i]}] = \exp\{-\Delta\mathcal{U}[\mathbf{s}_{[i-1,i]}, \mathbf{x}_{[i-1,i]}\}] = \mathcal{P}[\mathbf{x}_{[i-1,i]}|\mathbf{x}_{[0,i-1]}, \mathbf{s}_{[0,i]}]$  we generate normalized weights

$$W_i^k = \frac{\mathcal{P}[\mathbf{x}_{[i-1,i]}|\mathbf{x}_{[0,i-1]}, \mathbf{s}_{[0,i]}^k]}{\sum_{j=1}^M \mathcal{P}[\mathbf{x}_{[i-1,i]}|\mathbf{x}_{[0,i-1]}, \mathbf{s}_{[0,i]}^j]}, \quad (\text{A2})$$

cf. Eq. (A1). Note that this is the same choice of weighting function as in Section IIIB, Eq. (35). By comparison with the notation used there, we see that the Boltzmann factors  $U_i^k$  and Rosenbluth weights  $w_i$  were defined such that we can express the normalized weight equivalently as

$$W_i^k = \frac{e^{-U_i^k}}{w_i}. \quad (\text{A3})$$

Why is this choice of weighting function the correct one? First observe that resampling with the normalized weights from Eq. (A2) produces samples approximately distributed according to

$$\begin{aligned} h[\mathbf{s}_{[0,i]}] &= f[\mathbf{s}_{[0,i]}]g[\mathbf{s}_{[0,i]}] \\ &= \mathcal{P}[\mathbf{s}_{[0,i]}|\mathbf{x}_{[0,i-1]}] \mathcal{P}[\mathbf{x}_{[i-1,i]}|\mathbf{x}_{[0,i-1]}, \mathbf{s}_{[0,i]}]. \end{aligned} \quad (\text{A4})$$

What remains to be shown is that this density  $h[\mathbf{s}_{[0,i]}]$ , when normalized, becomes the desired target distribution  $\mathcal{P}[\mathbf{s}_{[0,i]}|\mathbf{x}_{[0,i]}]$ .

To do so, we need to rewrite the expression for

$g[\mathbf{s}_{[0,i]}] = \mathcal{P}[\mathbf{x}_{[i-1,i]}|\mathbf{x}_{[0,i-1]}, \mathbf{s}_{[0,i]}$  using Bayes' theorem

$$g[\mathbf{s}_{[0,i]}] = \frac{\mathcal{P}[\mathbf{s}_{[0,i]}|\mathbf{x}_{[0,i-1]}, \mathbf{x}_{[i-1,i]}] \mathcal{P}[\mathbf{x}_{[i-1,i]}|\mathbf{x}_{[0,i-1]}}{\mathcal{P}[\mathbf{s}_{[0,i]}|\mathbf{x}_{[0,i-1]}}. \quad (\text{A5})$$

Notice that the first term of the numerator can be written as  $\mathcal{P}[\mathbf{s}_{[0,i]}|\mathbf{x}_{[0,i]}]$ . After inserting this result into Eq. (A4) we obtain

$$h[\mathbf{s}_{[0,i]}] = \mathcal{P}[\mathbf{s}_{[0,i]}|\mathbf{x}_{[0,i]}] \mathcal{P}[\mathbf{x}_{[i-1,i]}|\mathbf{x}_{[0,i-1]}. \quad (\text{A6})$$

The second term in this product is a constant since  $\mathbf{x}$  is fixed. The first term is a normalized probability density for  $\mathbf{s}_{[0,i]}$ . Therefore we find that the normalized density corresponding to  $h[\mathbf{s}_{[0,i]}]$  is

$$\hat{h}[\mathbf{s}_{[0,i]}] = \mathcal{P}[\mathbf{s}_{[0,i]}|\mathbf{x}_{[0,i]}. \quad (\text{A7})$$

Consequently, this is the distribution that is approximated by the set of trajectories at the end of the  $i$ -th iteration of the particle filter, which is what we wanted to show. At its heart, the particle filter is therefore an algorithm to produce samples that are approximately distributed according to  $\mathcal{P}[\mathbf{s}|\mathbf{x}]$ .

### 3. Marginal Probability Estimate

We now use these insights to derive an estimate of the marginal density  $\mathcal{P}[\mathbf{x}]$ . We start by noting that the marginal density of the  $i$ -th output segment,  $\mathcal{P}[\mathbf{x}_{[i-1,i]}|\mathbf{x}_{[0,i-1]}]$ , is given by

$$\begin{aligned} & \mathcal{P}[\mathbf{x}_{[i-1,i]}|\mathbf{x}_{[0,i-1]}] \\ &= \int \mathcal{D}[\mathbf{s}_{[0,i]}] \mathcal{P}[\mathbf{x}_{[i-1,i]}, \mathbf{s}_{[0,i]}|\mathbf{x}_{[0,i-1]}] \\ &= \int \mathcal{D}[\mathbf{s}_{[0,i]}] \mathcal{P}[\mathbf{s}_{[0,i]}|\mathbf{x}_{[0,i-1]}] g[\mathbf{s}_{[0,i]}]. \end{aligned} \quad (\text{A8})$$

The third line follows from the definition of  $g[\mathbf{s}_{[0,i]}] = \mathcal{P}[\mathbf{x}_{[i-1,i]}|\mathbf{x}_{[0,i-1]}, \mathbf{s}_{[0,i]}]$ . Hence, we find that the probability  $\mathcal{P}[\mathbf{x}_{[i-1,i]}|\mathbf{x}_{[0,i-1]}]$  can be expressed as the average

$$\mathcal{P}[\mathbf{x}_{[i-1,i]}|\mathbf{x}_{[0,i-1]}] = \langle g[\mathbf{s}_{[0,i]}] \rangle_{\mathcal{P}[\mathbf{s}_{[0,i]}|\mathbf{x}_{[0,i-1]}}. \quad (\text{A9})$$

In principle, this average can be computed using a Monte Carlo scheme, using trajectories generated from  $\mathcal{P}[\mathbf{s}_{[0,i]}|\mathbf{x}_{[0,i-1]}]$ . Notice, that at each iteration of the particle filter, we *do* dispose of a set of trajectories  $\mathbf{s}_{[0,i]}^1, \dots, \mathbf{s}_{[0,i]}^M$  which are approximately distributed according to  $\mathcal{P}[\mathbf{s}_{[0,i]}|\mathbf{x}_{[0,i-1]}]$  above. Therefore, we can compute the average Eq. (A9) directly from the trajectories that are present for each iteration of the particle filter. With the notation from Section III B, using  $g[\mathbf{s}_{[0,i]}^k] = \exp(-U_i^k)$ , we thus obtain the estimate

$$\mathcal{P}[\mathbf{x}_{[i-1,i]}|\mathbf{x}_{[0,i-1]}] \approx \frac{1}{M} \sum_{k=1}^M e^{-U_i^k} = \frac{w_i}{M}. \quad (\text{A10})$$

The probability of the whole output trajectory  $\mathcal{P}[\mathbf{x}]$  is given by the product

$$\mathcal{P}[\mathbf{x}] = P(x_0) \mathcal{P}[\mathbf{x}_{[0,1]}|x_0] \cdots \mathcal{P}[\mathbf{x}_{[n-1,n]}|\mathbf{x}_{[0,n-1]}] \quad (\text{A11})$$

where  $P(x_0)$  is the probability of the initial output state  $x_0$  which is assumed to be known. Thus, we arrive at the following estimate for the marginal output probability

$$\hat{\mathcal{P}}[\mathbf{x}] = P(x_0) \prod_{i=1}^n \frac{w_i}{M} \quad (\text{A12})$$

which is precisely Eq. (38).

## Appendix B: MCMC Sampling in Trajectory Space

Thermodynamic Integration PWS in Section III C relies on computing averages with respect to  $\mathcal{P}_\theta[\mathbf{s}|\mathbf{x}] \propto \exp(-\mathcal{U}_\theta[\mathbf{s}, \mathbf{x}])$ . Sampling from these distributions using the SSA (Gillespie) algorithm is not possible. Instead, in this section we show different ways of how to implement a Markov Chain Monte Carlo (MCMC) sampler in trajectory space to generate correctly distributed trajectories.

We can build a MCMC sampler in trajectory space using the Metropolis-Hastings algorithm. To create a Markov Chain in trajectory space, we need to find a suitable proposal kernel, that generates a new trajectory  $\mathbf{s}'$  from a given trajectory  $\mathbf{s}$  with probability  $T(\mathbf{s} \rightarrow \mathbf{s}')$ . We accept the proposal using the Metropolis criterion with probability

$$A(\mathbf{s}', \mathbf{s}) = \min \left( 1, e^{\mathcal{U}_\theta[\mathbf{s}, \mathbf{x}] - \mathcal{U}_\theta[\mathbf{s}', \mathbf{x}]} \frac{T(\mathbf{s}' \rightarrow \mathbf{s})}{T(\mathbf{s} \rightarrow \mathbf{s}')} \right) \quad (\text{B1})$$

to create a chain of trajectories with stationary distribution given by  $\mathcal{P}_\theta[\mathbf{s}|\mathbf{x}] = e^{-\mathcal{U}_\theta[\mathbf{s}, \mathbf{x}]} / \mathcal{Z}_\theta[\mathbf{x}]$  for  $0 \leq \theta \leq 1$ . To ensure efficient convergence of the resulting Markov chain to its stationary distribution, the proposal kernel must balance two conflicting requirements. To efficiently explore the state space per unit amount of CPU time, the proposed trajectory  $\mathbf{s}'$  must be sufficiently different from the original trajectory  $\mathbf{s}$ , while at the same time it should not be so radically different that the acceptance probability is drastically reduced. Thus, the design of the proposal kernel is crucial for an efficient MCMC sampler and we will discuss various strategies to create trial trajectories. Since different types of trial moves can easily be combined in a Metropolis-Hastings algorithm, the most efficient samplers often incorporate multiple complementary proposal strategies to improve the exploration speed of the trajectory space.

The simplest (and naïve) proposal kernel is to just generate an entirely new trajectory  $\mathbf{s}'$  independent from  $\mathbf{s}$ , by sampling directly from  $\mathcal{P}[\mathbf{s}]$  using the SSA. Hence, the transition kernel is given by  $T(\mathbf{s} \rightarrow \mathbf{s}') = \mathcal{P}[\mathbf{s}']$  and

a proposal  $\mathbf{s} \rightarrow \mathbf{s}'$  is accepted with probability

$$\begin{aligned} A(\mathbf{s}', \mathbf{s}) &= \min \left( 1, e^{\mathcal{U}_\theta[\mathbf{s}, \mathbf{x}] - \mathcal{U}_\theta[\mathbf{s}', \mathbf{x}]} \frac{\mathcal{P}[\mathbf{s}]}{\mathcal{P}[\mathbf{s}']} \right) \\ &= \min \left( 1, \frac{\mathcal{P}[\mathbf{x}|\mathbf{s}']^\theta}{\mathcal{P}[\mathbf{x}|\mathbf{s}]^\theta} \right) \end{aligned} \quad (\text{B2})$$

where the second line follows by inserting the definition of  $\mathcal{U}_\theta[\mathbf{s}, \mathbf{x}]$  given in Eq. (41). While this simple scheme to completely regenerate an entire trajectory and accepting/rejecting according to  $A(\mathbf{s}', \mathbf{s})$  creates correctly distributed trajectories, it should not be used in simulations to compute  $\mathcal{P}[\mathbf{x}]$ . Indeed, we get a better estimate of  $\mathcal{P}[\mathbf{x}]$  by just using the same number of independent sample trajectories from  $\mathcal{P}[\mathbf{s}]$  and using the brute-force scheme in Eq. (8) without taking the detour of thermodynamic integration to estimate the normalization constant.

Instead, an idea from transition path sampling is to only regenerate a part of the old trajectory as part of the proposal kernel [98]. By not regenerating the entire trajectory, the new trajectory  $\mathbf{s}'$  is going to be correlated with the original trajectory  $\mathbf{s}$ , and correlation in general improves the acceptance rate. The simplest way to generate trial trajectories using a partial update is a move termed *forward shooting* in which a time point  $\tau$  along the existing trajectory  $\mathbf{s}$  is randomly selected, and a new trajectory segment is regrown from this point to the end, resulting in the proposal  $\mathbf{s}'$ . Since the new segment is generated according to the input statistics given by  $\mathcal{P}[\mathbf{s}_{[T-\tau, T]}]$ , the acceptance probability for the proposed trajectory is given by Eq. (B2). If the input dynamics given by  $\mathcal{P}[\mathbf{s}]$  are time-reversible, we can also perform a *backward shooting* move. Here, the beginning of  $\mathbf{s}$  is replaced by a new segment that is generated backwards in time. Assuming that the initial condition is the input's steady state distribution, the corresponding acceptance probability of the backward shooting move is again given by Eq. (B2). Using these two moves we create a MCMC sampler where both ends of the trajectory are flexible and thus if the trajectory is not too long, the chain will quickly relax to its stationary distribution. This is indeed the MCMC sampler used to obtain the TI-PWS results for the coupled birth-death process in Section V A.

For long trajectories it can prove to be a problem that the middle section is too inflexible when the proposal moves only regenerate either the beginning or the end of a trajectory. Therefore, one could additionally try to incorporate mid section regrowth to make sure that also the middle parts of the trajectory become flexible. To regrow a middle segment with duration  $\tau$  of a trajectory  $\mathbf{s}$ , we have to generate a new segment of duration  $\tau$  according to the stochastic dynamics given by  $\mathcal{P}[\mathbf{s}]$  but with the additional condition that we have to connect *both* endpoints of the new segment to the existing trajectory. While the starting point of the segment can be chosen freely, the challenge is to ensure that the endpoint of the new segment satisfies the end-point constraint. Stochastic processes that generate trajectories under the condi-

tion of hitting a specific point after a given duration  $\tau$  are called stochastic bridging processes.

The simplest way to generate trajectories from a bridging process is by generating a trajectory segment of length  $\tau$  from the normal stochastic process and rejecting the segment if it does not hit the correct end point [99]. Clearly, this strategy is only feasible for very short segments and when the state space is discrete, as otherwise almost every generated segment will be rejected due to not hitting the correct end point. To avoid this issue, more efficient algorithms have been developed to simulate stochastic bridges for some types of stochastic processes. For diffusion processes, bridges can be simulated efficiently by introducing a guiding term into the corresponding Langevin equation [100]. For jump processes, bridges can be simulated using a particle filters [101], by a weighted stochastic simulation algorithm (wSSA) [102], or using random time discretization [99].

Further techniques to create a trajectory space MCMC samplers have been developed in the literature. Crooks [103] describes a scheme to create MCMC moves for trajectories evolving in non-equilibrium dynamics, by making MCMC moves to change the trajectories' noise histories. In the Particle Markov Chain Monte Carlo (PMCMC) algorithm, proposal trajectories are generated using a particle filter and accepted with an appropriate Metropolis criterion [104]. Another class of efficient samplers for Markov jump processes can be built using uniformization [105].

### Appendix C: Dealing with Feedback

While so far, we have assumed the stochastic dynamics of the input to be independent of the generated output trajectories, in principle all physical information processing systems exhibit this kind of feedback. The physical interaction needed to measure the input signal necessarily affects the incoming signal, and indeed, it follows that no information can be extracted from the input signal without any perturbation of the input dynamics. Often, it is assumed that the amplitude of such perturbations is comparatively small and thus that the feedback can safely be ignored. Above, the PWS scheme was derived with this assumption. In this section we drop the assumption and will explicitly consider systems where the produced output perturbs the input, i.e. systems where the output feeds back onto the input. In the following we will first discuss the additional problems that arise when computing the mutual information for a system with feedback, and subsequently we present a modified version of PWS that can be used to compute the trajectory mutual information for these systems.

## 1. Computing the Mutual Information with Feedback between Input and Output

All PWS schemes presented above require the computation of the trajectory likelihood  $\mathcal{P}[\mathbf{x}|\mathbf{s}]$ , a quantity that is not readily available for systems with feedback. Indeed, as already mentioned in Section II C 1, for a given input trajectory  $\mathbf{s}$ , the output dynamics are no longer described by a Markov process in a system with feedback and therefore we cannot find an expression for  $\mathcal{P}[\mathbf{x}|\mathbf{s}]$  based on the master equation. This implies that for systems with feedback PWS schemes cannot be used without modification. While it is generally not possible to derive an expression for the conditional probability  $\mathcal{P}[\mathbf{x}|\mathbf{s}]$  in systems with feedback, we often still can compute the joint probability density  $\mathcal{P}[\mathbf{s}, \mathbf{x}]$  instead. Based on this quantity, we will present a modified PWS scheme to compute the mutual information for systems with feedback.

Specifically, since PWS is a model-based approach to compute the mutual information, when there is feedback from the output back to the input, we require a complete model of the combined system. Specifically, such a model must provide an expression for the joint probability  $\mathcal{P}[\mathbf{s}, \mathbf{x}]$ , describing the input dynamics and the interaction between input and output, including the feedback.

An estimate of the mutual information that only relies on the computation of joint probability densities  $\mathcal{P}[\mathbf{s}, \mathbf{x}]$  can be obtained by expressing the mutual information as

$$I(\mathcal{S}, \mathcal{X}) = \int \mathcal{D}[\mathbf{s}] \int \mathcal{D}[\mathbf{x}] \mathcal{P}[\mathbf{s}, \mathbf{x}] \ln \frac{\mathcal{P}[\mathbf{s}, \mathbf{x}]}{\mathcal{P}[\mathbf{s}] \mathcal{P}[\mathbf{x}]} \quad (\text{C1})$$

Thus, the PWS scheme with feedback consists of the computation of

$$I(\mathcal{S}, \mathcal{X}) = \left\langle \ln \frac{\mathcal{P}[\mathbf{s}, \mathbf{x}]}{\mathcal{P}[\mathbf{s}] \mathcal{P}[\mathbf{x}]} \right\rangle_{\mathcal{P}[\mathbf{s}, \mathbf{x}]} \quad (\text{C2})$$

which we want to estimate via a Monte Carlo average using samples from  $\mathcal{P}[\mathbf{s}, \mathbf{x}]$ . We see that while we don't need to evaluate the likelihood  $\mathcal{P}[\mathbf{x}|\mathbf{s}]$ , we now need to explicitly compute the joint density  $\mathcal{P}[\mathbf{s}, \mathbf{x}]$ , and two marginal densities,  $\mathcal{P}[\mathbf{s}]$  and  $\mathcal{P}[\mathbf{x}]$ , for each Monte Carlo sample  $(\mathbf{s}, \mathbf{x}) \sim \mathcal{P}[\mathbf{s}, \mathbf{x}]$ . While the joint density can be evaluated directly by assumption, each of the marginalized densities can only be computed using a nested Monte Carlo estimate.

Specifically, for PWS with feedback, we need to compute *two* marginalization integrals per Monte Carlo sample:

$$\mathcal{P}[\mathbf{s}] = \int \mathcal{D}[\mathbf{x}] \mathcal{P}[\mathbf{s}, \mathbf{x}], \quad (\text{C3})$$

and

$$\mathcal{P}[\mathbf{x}] = \int \mathcal{D}[\mathbf{s}] \mathcal{P}[\mathbf{s}, \mathbf{x}]. \quad (\text{C4})$$

However, these marginalization integrals cannot be directly computed with the techniques described so far.

Note that while in Section III we discussed in detail how to compute such marginalization integrals, all methods presented there themselves require the evaluation of the likelihood  $\mathcal{P}[\mathbf{x}|\mathbf{s}]$  and cannot be used directly. Therefore, in the following subsection we discuss how to compute marginalization integrals for systems with feedback.

Additionally, as discussed in Section IV, we may also need to integrate out internal components of the master equation even when the output feeds back onto these internal components. The technique discussed below can also be used in this case as a way to compute the marginalization integral in Eq. (45).

## 2. Marginalization Integrals for Systems with Feedback

Computing marginalization integrals in systems with feedback is harder than it is in the case without feedback. Specifically, we will show that it is not obvious how to apply the brute force Monte Carlo estimate Eq. (8) or the other, more advanced techniques from Section III A to systems with feedback. Nonetheless, if the system with feedback can be decomposed into a non-interacting part and an interacting part that includes the feedback, it is often still possible to compute marginalization integrals. Below, we sketch the steps that are necessary in order to compute marginalization integrals for systems with feedback using such a decomposition.

For concreteness, we discuss how to compute

$$\mathcal{P}[\mathbf{x}] = \int \mathcal{D}[\mathbf{s}] \mathcal{P}[\mathbf{s}, \mathbf{x}] \quad (\text{C5})$$

as the prototype for a marginalization integral we want to compute. In contrast to Section III A, we now assume that  $\mathbf{x}$  feeds back onto  $\mathbf{s}$ . That means, that we have access to the joint distribution's density  $\mathcal{P}[\mathbf{s}, \mathbf{x}]$ , but not to the marginal density  $\mathcal{P}[\mathbf{s}]$  or the conditional density  $\mathcal{P}[\mathbf{x}|\mathbf{s}]$ .

Formulated in the language of statistical physics, all of the techniques of Section III A are estimators of the free-energy difference  $\Delta\mathcal{F}[\mathbf{x}] = \mathcal{F}[\mathbf{x}] - \mathcal{F}_0[\mathbf{x}]$  between two ensembles described by potentials  $\mathcal{U}[\mathbf{s}, \mathbf{x}]$  and  $\mathcal{U}_0[\mathbf{s}, \mathbf{x}]$ . Previously, for systems without feedback, we chose these potentials to be  $\mathcal{U}_0[\mathbf{s}, \mathbf{x}] = -\ln \mathcal{P}[\mathbf{s}]$  and  $\mathcal{U}[\mathbf{s}, \mathbf{x}] = -\ln \mathcal{P}[\mathbf{s}, \mathbf{x}]$  with the idea that  $\mathcal{U}$  is the potential corresponding to the actual system and  $\mathcal{U}_0$  is the potential of a reference system with known free energy. Then, by computing the free-energy difference between the reference system and the actual system, we could compute the marginal probability  $\mathcal{P}[\mathbf{x}]$ .

However, in systems with feedback we face a problem. Note that the actual system is still described by the potential  $\mathcal{U}[\mathbf{s}, \mathbf{x}] = -\ln \mathcal{P}[\mathbf{s}, \mathbf{x}]$ , even with feedback. Yet, for the reference system described by  $\mathcal{U}_0[\mathbf{s}, \mathbf{x}]$  we cannot make the same choice as before, because the previous choice involved the marginal probability  $\mathcal{P}[\mathbf{s}]$  which is not available with feedback.

Instead, we have to find an alternative expression for  $\mathcal{U}_0[\mathbf{s}, \mathbf{x}]$ . To construct a suitable reference potential, we can use a decomposition of the full potential into three parts

$$\mathcal{U}[\mathbf{s}, \mathbf{x}] = \mathcal{U}_S[\mathbf{s}] + \mathcal{U}_X[\mathbf{x}] + \Delta\mathcal{U}[\mathbf{s}, \mathbf{x}] \quad (\text{C6})$$

where  $\Delta\mathcal{U}[\mathbf{s}, \mathbf{x}]$  describes the features of the system that induce interaction, or correlation, between  $\mathbf{s}$  and  $\mathbf{x}$ . The first two terms of the potential above,  $\mathcal{U}_S[\mathbf{s}] + \mathcal{U}_X[\mathbf{x}]$ , therefore describe a *non-interacting* version of the system, where the input and output are fully independent of each other. We want to use the potential of that non-interacting version as our expression for  $\mathcal{U}_0$ , i.e.  $\mathcal{U}_0[\mathbf{s}, \mathbf{x}] = \mathcal{U}_S[\mathbf{s}] + \mathcal{U}_X[\mathbf{x}]$ . To be able to do so, we require that the partition function (normalization constant)

$$\mathcal{Z}_0[\mathbf{x}] = \int \mathcal{D}[\mathbf{s}] e^{-\mathcal{U}_0[\mathbf{s}, \mathbf{x}]} \quad (\text{C7})$$

is known. In other words, we need to choose the decomposition in Eq. (C6) such that the partition function Eq. (C7) is known either analytically or numerically. If such a decomposition is found, we can compute the marginal probability  $\mathcal{P}[\mathbf{x}]$  from the free-energy difference  $\Delta\mathcal{F}[\mathbf{x}]$  between  $\mathcal{U}$  and  $\mathcal{U}_0$ :

$$-\ln \mathcal{P}[\mathbf{x}] = \mathcal{F}[\mathbf{x}] = \mathcal{F}_0[\mathbf{x}] + \Delta\mathcal{F}[\mathbf{x}] \quad (\text{C8})$$

where  $\mathcal{F}_0 = -\ln \mathcal{Z}_0[\mathbf{x}]$  is known. Because we have a known expression for  $\mathcal{U}_0[\mathbf{s}, \mathbf{x}]$ , the free-energy difference  $\Delta\mathcal{F}[\mathbf{x}]$  can now be computed using any of the techniques described in Section III A.

As an example for finding a decomposition like Eq. (C6), let us consider the case where the joint system of input and output is described by a single master equation, i.e. we have a master equation with two components,  $S$  which represents the input, and  $X$  which represents the output. In such a system, information is transmitted, if there exist transitions that change the copy number of  $X$  with a rate that is dependent on the copy number of  $S$ . In terms of chemical reactions,  $S \rightarrow S + X$  is an example for such a transition. In turn, this system exhibits feedback if at least one of the transitions that change the copy number of  $S$  has a rate that depends on  $X$ , as for example with the reaction  $S + X \rightarrow X$ . Note that with such reactions, the dynamics of  $S$  depend on the current copy number of  $X$ , and therefore we cannot evolve  $S$  trajectories independently of  $X$  trajectories, a consequence of feedback. Both of the reactions  $S \rightarrow S + X$  and  $S + X \rightarrow X$  introduce correlations between the  $S$  and  $X$  trajectories.

In a non-interacting system, such interactions between the input and output must be absent. Thus, a non-interacting version of the reaction system contains no single reaction that involves both  $S$  and  $X$ . We will now describe how we can use that non-interacting version of the reaction system, to obtain the reference potential  $\mathcal{U}_0[\mathbf{s}, \mathbf{x}]$ . Since the input and output trajectories are completely independent in the non-interacting

system, we can express the joint distribution's probability density as the product of the individual component's trajectory densities,  $\mathcal{P}_0[\mathbf{s}, \mathbf{x}] = \mathcal{P}_0[\mathbf{s}] \mathcal{P}_0[\mathbf{x}]$ . Note that  $\mathcal{P}_0[\mathbf{s}]$  and  $\mathcal{P}_0[\mathbf{x}]$  are not to be confused with the marginal probabilities  $\mathcal{P}[\mathbf{s}]$  and  $\mathcal{P}[\mathbf{x}]$  of the *interacting* version of the reaction system, which need to be computed using a marginalization integral. Since in the non-interacting version both,  $S$  and  $X$  obey independent dynamics which are characterized by individual master equations, both  $\mathcal{P}_0[\mathbf{s}]$  and  $\mathcal{P}_0[\mathbf{x}]$  can be individually computed using Eq. (14). Thus, in this case, the non-interacting potential is  $\mathcal{U}_0[\mathbf{s}, \mathbf{x}] = -\ln \mathcal{P}_0[\mathbf{s}] - \ln \mathcal{P}_0[\mathbf{x}]$  and, since the probability densities  $\mathcal{P}_0[\mathbf{s}]$  and  $\mathcal{P}_0[\mathbf{x}]$  are normalized, the corresponding partition function is  $\mathcal{Z}_0 = 1$ . Hence, for this reaction system, we can straightforwardly define a non-interacting version that can be used to obtain the reference potential  $\mathcal{U}_0[\mathbf{s}, \mathbf{x}]$ . Using the techniques described in Section III A, we can then compute the free-energy difference between  $\mathcal{U}_0[\mathbf{s}, \mathbf{x}]$  and  $\mathcal{U}[\mathbf{s}, \mathbf{x}] = -\ln \mathcal{P}[\mathbf{s}, \mathbf{x}]$ , where the latter potential describes the dynamics of the fully interacting system. Specifically, we can compute the marginal probabilities  $\mathcal{P}[\mathbf{s}]$ ,  $\mathcal{P}[\mathbf{x}]$  pertaining to the interacting system which are required for the mutual information estimate in Eq. (C2).

In summary, for systems with feedback we can compute marginalization integrals by specifying a reference potential  $\mathcal{U}_0[\mathbf{s}, \mathbf{x}]$  by finding a non-interacting version of the system. However, barring a decomposition into interacting and non-interacting potentials, there is generally not an unambiguous choice of the reference potential  $\mathcal{U}_0[\mathbf{s}, \mathbf{x}]$  to compute the marginal probability  $\mathcal{P}[\mathbf{x}]$ . Still, if a suitable expression for  $\mathcal{U}_0[\mathbf{s}, \mathbf{x}]$  can be found, we can make use of the techniques developed in Section III A to compute marginal probability  $\mathcal{P}[\mathbf{x}]$ . Thus, the specific choice of  $\mathcal{U}_0[\mathbf{s}, \mathbf{x}]$  is system-specific.

#### Appendix D: Mutual Information using the Linear Noise Approximation

The trajectory mutual information can be computed analytically for purely Gaussian systems. In a Gaussian system, the probability of a (time-discretized) trajectory  $\mathbf{x} = [x(t_1), \dots, x(t_N)]^T$  is given by

$$\mathcal{P}[\mathbf{x}] = \frac{1}{(2\pi)^N |C|^{1/2}} \exp\left(-\frac{1}{2} \mathbf{x}^T C^{-1} \mathbf{x}\right). \quad (\text{D1})$$

The elements of the matrix  $C$  are given in terms of the system's steady-state correlation function:  $C_{ij} = C(t_i - t_j)$ . In Ref. [106] it is shown that the mutual information for a Gaussian system can be computed using

$$I(\mathcal{S}, \mathcal{X}) = \frac{1}{2} \ln \left[ \frac{|C^{ss}| |C^{xx}|}{|Z|} \right] \quad (\text{D2})$$

with

$$Z = \begin{pmatrix} C^{ss} & C^{sx} \\ C^{sx} & C^{xx} \end{pmatrix}. \quad (\text{D3})$$

Here  $C^{ss}$  and  $C^{xx}$  are the (auto-)correlation matrices of the input and the output, respectively, whereas  $C^{sx}$  and  $C^{xs}$  are obtained from the corresponding cross-correlation functions. In summary, for Gaussian systems the mutual information can be computed directly from the system's correlation functions.

Further, a well-defined procedure to obtain a Gaussian approximation of a system described by a chemical master equation is the *linear noise approximation* (LNA) [107]. The LNA yields a Gaussian description of a stochastic system in terms of a Langevin equation

$$\frac{d\mathbf{n}(t)}{dt} = \mathbf{A}\mathbf{n}(t) + \mathbf{B}\boldsymbol{\eta}(t) \quad (\text{D4})$$

where  $\mathbf{n}(t)$  is the vector of copy numbers and  $\boldsymbol{\eta}(t)$  is a vector of independent Gaussian white noise components with unit covariance. The LNA is essentially a procedure to obtain the matrices  $A$  and  $B$  from a master equation and described in detail in Ref. [107].

From the LNA description we can obtain the steady-state covariance matrix  $\Sigma$  for fluctuations in the copy numbers as the solution of the Lyapunov equation

$$\mathbf{A}\Sigma + \Sigma\mathbf{A}^T + \mathbf{B}\mathbf{B}^T = 0. \quad (\text{D5})$$

In steady-state, the correlation functions are then given by

$$C(\tau) = \begin{cases} e^{\mathbf{A}\tau\Sigma} & \text{for } \tau \geq 0 \\ \Sigma e^{-\mathbf{A}^T\tau} & \text{for } \tau < 0 \end{cases}. \quad (\text{D6})$$

With this result, the trajectory mutual information for a Gaussian system can be computed directly using Eq. (D2).

### Appendix E: Stochastic Chemotaxis Model

We developed a stochastic model for chemotaxis, describing the individual reactions at the level of a master equation. Hence, we consider the interactions between ligand and receptors, as well as the capacity of receptors to phosphorylate CheY via the receptor-associated kinase CheA. Phosphorylated CheY can bind to the molecular motors driving the flagella, thereby altering the cell's tumbling rate, but we do not model this. Additionally, we model the methylation dynamics of each receptor which affect the affinity of ligand binding and the kinase activity.

Receptors are organized in clusters on the cell surface. In our model, each cluster consists of 3 receptors. The ligand binding dynamics to a cluster is cooperative, and in spirit of the Monod-Wyman-Changeux (MWC) model [81, 108] we model this cooperativity by coupling the ligand-binding dynamics to conformational switching dynamics of the receptors. Specifically, each receptor can be in an active or in an inactive conformational state. Moreover, the energetic cost of two receptors in the same

cluster being in different conformational states is prohibitively large. This means that all receptors within a cluster switch conformation in concert, so that we can meaningfully speak of an active or an inactive cluster. Detailed balance requires that the ligand binding affinity depends on whether a cluster is in the active or inactive state. Consequently, we have a dissociation constant  $K_a$  for a ligand bound to an active receptor and another dissociation constant  $K_i$  for a ligand bound to an inactive receptor. For chemotaxis,  $K_a \gg K_i$ , i.e. the ligand binding affinity is higher for the inactive state.

Additionally, each receptor has a number of methylation sites (we assume 3 methylation sites per receptor) which affect the cluster's probability to be active, and allows the system to adapt to different ambient ligand concentrations. Methyl groups can be attached to a receptor by the protein CheR and are removed by the protein CheB. We model the receptors' methylation dynamics following the model of Barkai and Leibler [77], where CheB can only demethylate active receptors. Additionally, to ensure exact adaptation, in our model CheR can only attach methyl groups to inactive receptors, as in Ref. [109]. Further, we consider the concentrations of CheR and CheB constant and we describe the methylation dynamics via zero order dynamics, i.e. there is a constant rate  $k_R$  at which a methyl group is attached to an inactive cluster (which is independent of the number of remaining unoccupied methylation site) as well as a constant rate  $k_B$  at which a methyl group is removed from an active cluster (independent of the number of occupied methylation sites). Naturally, if all methylation sites of a cluster are (un)occupied, no further (de)methylation can happen.

parameter	value	description
$\langle [L] \rangle$	50 $\mu\text{M}$	mean ligand concentration
$N_{\text{clusters}}$	800	number of receptor clusters
$N_{\text{CheY}}$	10 000	number of total CheY proteins
$K_a$	500 $\mu\text{M}$	ligand dissociation constant of active receptors
$K_i$	25 $\mu\text{M}$	ligand dissociation constant of inactive receptors
$k_{\ell+}$	0.20 $\text{s}^{-1}\mu\text{M}^{-1}$	ligand binding rate
$k_R$	0.10 $\text{s}^{-1}$	methylation rate
$k_B$	0.10 $\text{s}^{-1}$	demethylation rate
$k_A$	$3.57 \times 10^{-3} \text{ s}^{-1}$	phosphorylation rate
$k_Z$	8.57 $\text{s}^{-1}$	dephosphorylation rate
$E_0$	3.0	free energy of unmethylated active cluster
$\delta f$	-1.5	free energy change of active conformation from attachment of one methyl group

TABLE II. Parameters used for chemotaxis model. Energies (last two rows) are given in multiples of  $k_B T$ .



In the MWC model, the overall probability for a cluster in a given configuration to be active is described by the effective free-energy difference between the active and inactive state of a receptor cluster which is given by

$$\Delta F(\ell, m) = E_0 + \ell \delta g + m \delta f \quad (\text{E1})$$

where  $E_0$  is the free-energy difference for a cluster with no ligands and no methyl groups attached. Further,  $\ell$  denotes the total number of ligands that are bound to receptors in the cluster and  $m$  denotes the total number of occupied methylation sites of all receptors in the cluster. Thus,  $\delta g$  and  $\delta f$  denote the change in free energy for a ligand binding or a methylation event, respectively. Since ligand binding happens in equilibrium,  $\delta g$  is given by

$$\delta g = \ln \frac{K_a}{K_i} \quad (\text{E2})$$

(in units of  $k_B T$ ) and since  $K_a \gg K_i \Rightarrow \delta g > 0$  we see that ligand binding favors the inactive state. At the same time, for chemotaxis  $\delta f < 0$  such that methylation favors the active state. The probability for a cluster with  $\ell$  bound ligands,  $m$  times methylated, to be in the active state according to the MWC model is

$$p_a(\ell, m) = \frac{1}{1 + e^{\Delta F(\ell, m)}}. \quad (\text{E3})$$

Since the timescale of conformational switching of active and inactive receptors is much faster than the timescale of ligand binding or methylation, we don't explicitly model reactions between active and inactive clusters to save computational effort. Thus, the state of each cluster is determined by two numbers  $(\ell, m)$ , the number of bound ligands and the number of occupied methylation sites. In our Gillespie simulation each possible state of a cluster is its own species, i.e. we have species  $C_{\ell, m}$  for  $\ell = 0, \dots, 3$  and  $m = 0, \dots, 9$ . Overall, our chemotaxis model consists of reactions describing a) the birth-death process that characterizes the ligand concentration, b) ligand-receptor binding, c) reactions describing the methylation dynamics of receptors, and d) phosphorylation and dephosphorylation of CheY mediated by active clusters.

The input ligand concentration is modeled as a simple birth-death process  $\emptyset \rightleftharpoons L$  with a constant birth rate  $\kappa$  and a constant decay rate  $\mu$ . This creates an input signal where the mean copy number  $\bar{L} = \kappa/\mu$  equals the variance of the copy number, i.e.  $\bar{L} = \sigma_L^2$ . For *E. coli* moving in a steep exponential ligand gradient, we assume a relative noise strength of  $\sigma_L/\bar{L} = 0.14$  [52, 85], resulting in  $\bar{L} = 50$ . The ratio between birth and decay rate is given by the mean ligand copy number  $\bar{L}$ , and the decay rate is determined by the input timescale  $\mu = 1/\tau_L$ . Additionally we use an ad-hoc mapping between the ligand copy number  $L(t)$  and the ligand concentration  $[L](t)$  given by

$$[L](t) = c_0 L(t) \quad (\text{E4})$$

with  $c_0 = 1.0 \mu\text{M}$ . I.e. each copy of  $L$  contributes  $c_0$  to the ligand concentration. Hence, the mean ligand concentration in our model is  $\langle [L] \rangle = c_0 \bar{L} = 50 \mu\text{M}$ .

For ligand-receptor interactions, we assume the rate of ligand binding  $C_{\ell, m} \rightarrow C_{\ell+1, m}$  is given by

$$k_{\ell+} [L](t) \quad (\text{E5})$$

i.e. the ligand binding rate is independent of the activity of a cluster. In contrast, the unbinding rates differ between the active and inactive conformations of a cluster and are determined by the dissociation constants  $K_a, K_i$  for the active and inactive state, respectively. Since we don't explicitly model the activity state of individual clusters, we use the probability of a cluster being active to determine the ligand unbinding rate  $C_{\ell, m} \rightarrow C_{\ell-1, m}$ :

$$k_{\ell-}(\ell, m) = k_{\ell+} [p_a(\ell, m)K_a + (1 - p_a(\ell, m))K_i]. \quad (\text{E6})$$

In a similar fashion, the methylation rate for  $C_{\ell, m} \rightarrow C_{\ell, m+1}$  is given by

$$k_{m+}(\ell, m) = (1 - p_a(\ell, m))k_R \quad (\text{E7})$$

and the demethylation rate for  $C_{\ell, m} \rightarrow C_{\ell, m-1}$  is given by

$$k_{m-}(\ell, m) = p_a(\ell, m)k_B. \quad (\text{E8})$$

These zero-order dynamics of (de)methylation of receptors lead to the adaptive behavior of the chemotaxis system. To see this we can express the change of average methylation level  $m(t)$  in a mean-field fashion by

$$\frac{dm(t)}{dt} = (1 - a(t))k_R - a(t)k_B \quad (\text{E9})$$

where  $a(t)$  is the mean-field cluster activity. Taking  $dm(t)/dt = 0$ , we find an adapted activity

$$a^* = \frac{k_R}{k_R + k_B} \quad (\text{E10})$$

which is independent of the ligand concentration. Hence, on the methylation time scale, the average activity relaxes to  $a^*$ . While this adapted activity is computed from a mean-field approximation, we find that in simulations of our stochastic model, the average activity reliably relaxes to  $a^*$  for a wide range of ligand concentrations.

Finally, we consider the dynamics of the phosphorylation of CheY. Only active receptors can phosphorylate the CheY protein using the receptor-associated kinase CheA, therefore we model phosphorylation as a reaction  $\text{CheY} + C_{\ell, m} \rightarrow \text{CheY-P} + C_{\ell, m}$  with a kinetic rate

$$k_{Y \rightarrow Y_P}(\ell, m) = p_a(\ell, m)k_A \quad (\text{E11})$$

where  $k_A$  is a constant that represents the phosphorylation rate of an active cluster. The dephosphorylation  $\text{CheY-P} \rightarrow \text{CheY}$  is carried out by a phosphatase CheZ which is assumed to happen at a constant rate  $k_Z$ .

For our simulations, we chose parameters to achieve (almost) perfect adaptation on a timescale comparable to experimental evidence (see Table II for a listing of all parameters). We model a system of 800 receptor clusters (2400 receptors), each of which can be in one of 40 states  $C_{\ell,m}$  for  $\ell = 0, \dots, 3$  and  $m = 0, \dots, 9$ . The dissociation constants  $K_a, K_i$  are chosen based on physiological values for Tar receptors binding the attractant  $\alpha$ -methylaspartate (MeAsp) [110]. For simplicity we set the (de)methylation rates to be equal,  $k_B = k_R$ , which results in an adapted activity of  $a^* = 0.5$ . The free energy  $\delta f$  associated with methylation is chosen such that the addition of two methyl groups to a cluster roughly counterbalances the free energy increase of binding an additional ligand (i.e.  $2\delta f + \delta g \approx 0$ ).  $E_0$  is chosen such that for zero ligand concentration, each cluster is on average twice methylated. The remaining parameters were chosen by considering the typical time scales of chemotaxis.

The ligand binding dynamics have a relaxation time on the order of  $\approx 0.01$  s. Ligand unbinding in the active state happens on the time scale of

$$\tau_\ell = [k_{\ell+} (\langle [L] \rangle + K_a)]^{-1} \quad (\text{E12})$$

and by setting this timescale  $\tau_\ell = 0.01$  s we obtain the

ligand binding rate  $k_{\ell+}$ .

These fast ligand binding/unbinding events are averaged out by the slower phosphorylation dynamics of CheY on the order of  $\approx 0.1$  s [88]. For our model, we define the phosphorylation time scale as

$$\tau_Y = (k_A a^* N_{\text{clusters}} + k_Z)^{-1} \quad (\text{E13})$$

where the term  $(k_A a^* N_{\text{clusters}})$  represents the average rate of phosphorylation in the fully adapted chemotaxis network. Additionally, we assume that for the fully adapted system, roughly 1/6 of all CheY proteins are phosphorylated [88]. This allows us to obtain the parameter values for  $k_A$  and  $k_Z$ .

Finally, the slowest time scale is the methylation time scale  $\approx 10$  s which is the time scale of chemotactic adaptation. We approximate the methylation timescale by linearizing and solving Eq. (E9) to find the expression

$$\tau_m = \frac{1}{(-\delta f)k_B a^*} \quad (\text{E14})$$

from which we can obtain the (de)methylation rates  $k_B$  and  $k_R$  using the constraint  $k_B = k_R$ .

- 
- [1] G. Tkačik and A. M. Walczak, *Journal of Physics: Condensed Matter* **23**, 153102 (2011), 1101.4240.
  - [2] G. Tkačik and W. Bialek, *Annual Review of Condensed Matter Physics* **7**, 89 (2016).
  - [3] D. MacKay, *Information theory, inference, and learning algorithms* (Cambridge University Press, Cambridge, UK, 2003).
  - [4] C. E. Shannon, *Bell System Technical Journal* **27**, 379 (1948).
  - [5] T. M. Cover and J. A. Thomas, *Elements of Information Theory*, 2nd ed. (John Wiley & Sons, 2006).
  - [6] F. Tostevin and P. R. ten Wolde, *Physical Review Letters* **102**, 218101 (2009), 0901.0280.
  - [7] P. Fiedor, *Physical Review E* **89**, 052801 (2014), 1401.2548.
  - [8] J. Massey, *Proceedings of the International Symposium on Information Theory and its Applications.*, 303–305 (1990).
  - [9] T. Schreiber, *Physical Review Letters* **85**, 461 (2000), nlin/0001042.
  - [10] S. M. Block, J. E. Segall, and H. C. Berg, *Journal of Bacteriology* **154**, 312 (1983).
  - [11] J. E. Segall, S. M. Block, and H. C. Berg, *Proceedings of the National Academy of Sciences* **83**, 8987 (1986).
  - [12] C. Marshall, *Cell* **80**, 179 (1995).
  - [13] J. Purvis and G. Lahav, *Cell* **152**, 945 (2013).
  - [14] J. Selimkhanov, B. Taylor, J. Yao, A. Pilko, J. Albeck, A. Hoffmann, L. Tsimring, and R. Wollman, *Science* **346**, 1370 (2014).
  - [15] A. A. Granados, J. M. J. Pietsch, S. A. Cepeda-Humerez, I. L. Farquhar, G. Tkačik, and P. S. Swain, *Proceedings of the National Academy of Sciences* **115**, 201716659 (2018).
  - [16] S. P. Strong, R. Koberle, R. R. de Ruyter van Steveninck, and W. Bialek, *Physical Review Letters* **80**, 197 (1998).
  - [17] L. Paninski, *Neural Computation* **15**, 1191 (2003).
  - [18] R. Cheong, A. Rhee, C. J. Wang, I. Nemenman, and A. Levchenko, *Science* **334**, 354 (2011).
  - [19] G. Tkačik, C. G. Callan, and W. Bialek, *Proceedings of the National Academy of Sciences* **105**, 12265 (2008), 0705.0313.
  - [20] G. Tkačik, J. O. Dubuis, M. D. Petkova, and T. Gregor, *Genetics* **199**, genetics.114.171850 (2014).
  - [21] M. Meijers, S. Ito, and P. R. ten Wolde, *Physical Review E* **103**, L010102 (2021), 1906.00787.
  - [22] F. Rieke, D. Warland, R. d. R. v. Steveninck, and W. Bialek, *Spikes: exploring the neural code* (MIT Press, Cambridge, Massachusetts, 1999).
  - [23] A. Kaiser and T. Schreiber, *Physica D: Nonlinear Phenomena* **166**, 43 (2002).
  - [24] A. Kraskov, H. Stögbauer, and P. Grassberger, *Physical Review E* **69**, 066138 (2004), cond-mat/0305641.
  - [25] S. A. Cepeda-Humerez, J. Ruess, and G. Tkačik, *PLoS computational biology* **15**, e1007290 (2019).
  - [26] P. J. Thomas and A. W. Eckford, *IEEE Transactions on Information Theory* **62**, 7358 (2016), 1305.2245.
  - [27] Y. Gao, I. Kontoyiannis, and E. Bienenstock, *Entropy* **10**, 71 (2008), 0802.4363.
  - [28] A. Borst and F. E. Theunissen, *Nature Neuroscience* **2**, 947 (1999).
  - [29] M. Hledík, T. R. Sokolowski, and G. Tkačik, in *2019*

- IEEE Information Theory Workshop (ITW)* (2019) pp. 1–5.
- [30] L. Duso and C. Zechner, in *2019 IEEE 58th Conference on Decision and Control (CDC)* (IEEE, Piscataway, N.J., 2019) pp. 6610–6615, 1904.01988.
- [31] M. Delbrück, *The Journal of Chemical Physics* **8**, 120 (1940).
- [32] D. A. McQuarrie, *The Journal of Chemical Physics* **38**, 433 (1963).
- [33] D. A. McQuarrie, C. J. Jachimowski, and M. E. Russell, *The Journal of Chemical Physics* **40**, 2914 (1964).
- [34] M. B. Elowitz and S. Leibler, *Nature* **403**, 335 (2000).
- [35] W. Feller, *Acta Biotheoretica* **5**, 11 (1939).
- [36] J.-M. Park, E. Muñoz, and M. W. Deem, *Physical Review E* **81**, 011902 (2010), 1002.3837.
- [37] J. Cremer, A. Melbinger, and E. Frey, *Scientific Reports* **2**, 281 (2012), 1203.5863.
- [38] W. Weidlich and M. Braun, *Journal of Evolutionary Economics* **2**, 233 (1992).
- [39] T. Lux, *The Economic Journal* **105**, 881 (1995).
- [40] D. Helbing, *Reviews of Modern Physics* **73**, 1067 (2001), cond-mat/0012229.
- [41] C. Castellano, S. Fortunato, and V. Loreto, *Reviews of Modern Physics* **81**, 591 (2009), 0710.3256.
- [42] J. I. Siepmann, *Molecular Physics* **70**, 1145 (1990).
- [43] P. Grassberger, *Physical Review E* **56**, 3682 (1997).
- [44] D. Frenkel and B. Smit, *Understanding Molecular Simulation*, 2nd ed. (Academic Press, San Diego, 2002).
- [45] D. Frenkel and A. J. C. Ladd, *The Journal of Chemical Physics* **81**, 3188 (1984).
- [46] A. Gelman and X.-L. Meng, *Statistical Science* **13**, 163 (1998).
- [47] R. M. Neal, *Statistics and Computing* **11**, 125 (2001).
- [48] P. G. Bolhuis, D. Chandler, C. Dellago, and P. L. Geissler, *Annual Review of Physical Chemistry* **53**, 291 (2002).
- [49] L. E. Baum and T. Petrie, *The Annals of Mathematical Statistics* **37**, 1554 (1966).
- [50] L. Paninski, Y. Ahmadian, D. G. Ferreira, S. Koyama, K. R. Rad, M. Vidne, J. Vogelstein, and W. Wu, *Journal of Computational Neuroscience* **29**, 107 (2010).
- [51] Y. Tang, A. Adelaja, F. X.-F. Ye, E. Deeds, R. Wollman, and A. Hoffmann, *Nature Communications* **12**, 1272 (2021).
- [52] H. H. Mattingly, K. Kamino, B. B. Machta, and T. Emonet, *Nature Physics* **17**, 1426 (2021).
- [53] N. G. van Kampen, *Stochastic Processes in Physics and Chemistry*, 3rd ed. (Elsevier, Amsterdam, 2007).
- [54] M. F. Weber and E. Frey, *Reports on Progress in Physics* **80**, 046601 (2017), 1609.02849.
- [55] A. M. Walczak, A. Mugler, and C. H. Wiggins, *Proceedings of the National Academy of Sciences* **106**, 6529 (2009), 0811.4149.
- [56] K.-Y. Kim and J. Wang, *PLoS Computational Biology* **3**, e60 (2007).
- [57] D. T. Gillespie, *Journal of Computational Physics* **22**, 403 (1976).
- [58] A. Prados, J. J. Brey, and B. Sánchez-Rey, *Journal of Statistical Physics* **89**, 709 (1997).
- [59] V. H. Thanh and C. Priami, *The Journal of Chemical Physics* **143**, 054104 (2015).
- [60] P. E. Kloeden and E. Platen, *Numerical Solution of Stochastic Differential Equations* (Springer, Berlin, Heidelberg, 1992).
- [61] Indeed, the mutual information  $I(\mathcal{S}, \mathcal{X})$  precisely quantifies how strong the statistical dependence is between the trajectory-valued random variables  $\mathcal{S}$  and  $\mathcal{X}$ . From its definition  $I(\mathcal{S}, \mathcal{X}) = H(\mathcal{S}) - H(\mathcal{S}|\mathcal{X})$  we can understand more clearly how this affects the efficiency of the Monte Carlo estimate. Roughly speaking,  $H(\mathcal{S})$  is related to the number of distinct trajectories  $\mathbf{s}$  that can arise from the dynamics given by  $\mathcal{P}[\mathbf{s}]$ , while  $H(\mathcal{S}|\mathcal{X})$  is related to the number of distinct trajectories  $\mathbf{s}$  that could have led to a specific output  $\mathbf{x}$ , on average. Therefore, if the mutual information is very large, the difference between these two numbers is very large, and consequently the number of overall distinct trajectories is much larger than the number of distinct trajectories compatible with output  $\mathbf{x}$ . Now, if we generate trajectories according to the dynamics given by  $\mathcal{P}[\mathbf{s}]$ , with overwhelming probability we generate a trajectory  $\mathbf{s}$  which is not compatible with the output trajectory  $\mathbf{x}$ , and therefore  $\mathcal{P}[\mathbf{x}|\mathbf{s}] \approx 0$ . Hence, the effective number of samples  $M_{\text{eff}}$  is much smaller than the actual number of generated trajectories  $M$ , i.e.  $M_{\text{eff}} \ll M$ . We therefore only expect the estimate in Eq. (8) to be reliable when computing the mutual information for systems where it is not too high. Thus, strikingly, the difficulty of computing the mutual information is proportional to the magnitude of the mutual information itself.
- [62] M. Müller and W. Paul, *The Journal of Chemical Physics* **100**, 719 (1994).
- [63] M. N. Rosenbluth and A. W. Rosenbluth, *The Journal of Chemical Physics* **23**, 356 (1955).
- [64] N. J. Gordon, D. J. Salmond, and A. F. M. Smith, *IEE Proceedings F Radar and Signal Processing* **140**, 107 (1993).
- [65] T. Prellberg and J. Krawczyk, *Physical Review Letters* **92**, 120602 (2004).
- [66] R. J. Allen, D. Frenkel, and P. R. ten Wolde, *The Journal of Chemical Physics* **124**, 024102 (2006), cond-mat/0509499.
- [67] N. B. Becker, R. J. Allen, and P. R. ten Wolde, *The Journal of Chemical Physics* **136**, 174118 (2012), 1201.3823.
- [68] L. Martino, V. Elvira, and F. Louzada, *Signal Processing* **131**, 386 (2017), 1602.03572.
- [69] A. Doucet and A. M. Johansen, in *Oxford Handbook of Nonlinear Filtering*, edited by D. Crisan and B. Rozovskii (Oxford University Press, 2011).
- [70] N. Metropolis, A. W. Rosenbluth, M. N. Rosenbluth, A. H. Teller, and E. Teller, *The Journal of Chemical Physics* **21**, 1087 (1953).
- [71] J. Bezanson, A. Edelman, S. Karpinski, and V. B. Shah, *SIAM Review* **59**, 65 (2017).
- [72] M. Reinhardt, *PathWeightSampling.jl* (v0.1.0) (2021), Zenodo; manuel-rhdt/PathWeightSampling.jl, GitHub.
- [73] C. Rackauckas and Q. Nie, *Journal of Open Research Software* **5**, 15 (2017).
- [74] Y. Ma, S. Gowda, R. Anantharaman, C. Laughman, V. Shah, and C. Rackauckas, arXiv (2021), 2103.05244.
- [75] <https://github.com/zechnerlab/PathMI/tree/302f03e51ad195adc6be39fa9618886c76590cc4>.
- [76] H. Berg and E. Purcell, *Biophysical Journal* **20**, 193 (1977).
- [77] N. Barkai and S. Leibler, *Nature* **387**, 913 (1997).
- [78] R. G. Endres and N. S. Wingreen, *Proceedings of the National Academy of Sciences* **103**, 13040 (2006).

- [79] G. Lan, P. Sartori, S. Neumann, V. Sourjik, and Y. Tu, *Nature Physics* **8**, 422 (2012).
- [80] P. Sartori and Y. Tu, *Physical Review Letters* **115**, 118102 (2015), 1505.07413.
- [81] J. Monod, J. Wyman, and J.-P. Changeux, *Journal of Molecular Biology* **12**, 88 (1965).
- [82] N. B. Becker, A. Mugler, and P. R. ten Wolde, *Physical Review Letters* **115**, 258103 (2015).
- [83] R. A. Brittain, N. S. Jones, and T. E. Ouldridge, *Journal of Statistical Mechanics: Theory and Experiment* **2017**, 063502 (2017), 1702.06041.
- [84] S. G. Das, M. Rao, and G. Iyengar, *Physical Review E* **95**, 062410 (2017), 1608.07663.
- [85] G. Malaguti and P. R. ten Wolde, *eLife* **10**, e62574 (2021).
- [86] H. C. Berg and D. A. Brown, *Nature* **239**, 500 (1972).
- [87] K. Taute, S. Gude, S. Tans, and T. Shimizu, *Nature Communications* **6**, 8776 (2015).
- [88] V. Sourjik and H. C. Berg, *Proceedings of the National Academy of Sciences* **99**, 12669 (2002).
- [89] E. A. Korobkova, T. Emonet, H. Park, and P. Cluzel, *Physical review letters* **96**, 058105 (2006).
- [90] J. E. Segall, M. D. Manson, and H. C. Berg, *Nature* **296**, 855 (1982).
- [91] L. Onsager and S. Machlup, *Physical Review* **91**, 1505 (1953).
- [92] A. B. Adib, *The Journal of Physical Chemistry B* **112**, 5910 (2008), 0712.1255.
- [93] J. I. Siepmann and D. Frenkel, *Molecular Physics* **75**, 59 (1992).
- [94] T. S. van Erp, D. Moroni, and P. G. Bolhuis, *The Journal of Chemical Physics* **118**, 7762 (2003), cond-mat/0210614.
- [95] T. J. H. Vlugt and B. Smit, *PhysChemComm* **4**, 11 (2001).
- [96] P. Del Moral, *Comptes Rendus de l'Académie des Sciences - Series I - Mathematics* **325**, 653 (1997).
- [97] A. F. M. Smith and A. E. Gelfand, *The American Statistician* **46**, 84 (1992).
- [98] C. Dellago, P. G. Bolhuis, and D. Chandler, *The Journal of Chemical Physics* **108**, 9236 (1998).
- [99] A. Hobolth and E. A. Stone, *The Annals of Applied Statistics* **3**, 1204 (2009), 0910.1683.
- [100] F. van der Meulen and M. Schauer, *Electronic Journal of Statistics* **11**, 2358 (2017), 1406.4704.
- [101] A. Golightly and D. J. Wilkinson, *Statistical Applications in Genetics and Molecular Biology* **14**, 169 (2015).
- [102] C. S. Gillespie and A. Golightly, *The Journal of Chemical Physics* **150**, 224103 (2019).
- [103] G. E. Crooks, *Physical Review E* **61**, 2361 (2000), cond-mat/9908420.
- [104] C. Andrieu, A. Doucet, and R. Holenstein, *Journal of the Royal Statistical Society: Series B (Statistical Methodology)* **72**, 269 (2010).
- [105] V. Rao and Y. W. Teh, *Journal of Machine Learning Research* **14**, 3295 (2013).
- [106] F. Tostevin and P. R. ten Wolde, *Physical Review E* **81**, 061917 (2010), 1002.4273.
- [107] C. Gardiner, *Stochastic Methods*, 4th ed., Springer Series in Synergetics No. 13 (Springer-Verlag, Berlin Heidelberg, 2009).
- [108] V. Sourjik and H. C. Berg, *Nature* **428**, 437 (2004).
- [109] C. J. Morton-Firth, T. S. Shimizu, and D. Bray, *Journal of Molecular Biology* **286**, 1059 (1999).
- [110] J. E. Keymer, R. G. Endres, M. Skoge, Y. Meir, and N. S. Wingreen, *Proceedings of the National Academy of Sciences* **103**, 1786 (2006).